Ann. Inst. H. Poincaré D
Comb. Phys. Interact. (Online first)
DOI 10.4171/AIHPD/163

Cube moves for s-embeddings and α-realizations

Paul Melotti, Sanjay Ramassamy, and Paul Thévenin

Abstract. Chelkak introduced s-embeddings as tilings by tangential quads which provide the right setting to study the Ising model with arbitrary coupling constants on arbitrary planar graphs. We prove the existence and uniqueness of a local transformation for s-embeddings called the cube move, which consists in flipping three quadrilaterals in such a way that the resulting tiling is also in the class of s-embeddings. In passing, we give a new and simpler formula for the change in coupling constants for the Ising star-triangle transformation which is conjugated to the cube move for s-embeddings. We introduce more generally the class of α-embeddings as tilings of a portion of the plane by quadrilaterals such that the side lengths of each quadrilateral $ABCD$ satisfy the relation $AB^\alpha + CD^\alpha = AD^\alpha + BC^\alpha$, providing a common generalization for harmonic embeddings adapted to the study of resistor networks ($\alpha = 2$) and for s-embeddings ($\alpha = 1$). We investigate existence and uniqueness properties of the cube move for these α-embeddings.

1. Introduction

The star-triangle transformation was first introduced by Kennelly in the context of resistor networks [16] as a local transformation which does not change the electrical properties of the network (such as the equivalent resistance) outside of the location where the transformation is performed. It consists in replacing a vertex of degree 3 by a triangle as in Figure 1, and the conductances after the transformation are given as some rational functions of the conductances before the transformation. It follows from the classical connection between resistor networks and random walks [15] that applying this star-triangle transformation to a graph with weights on the edges also preserves the probabilistic properties of the random walk on this graph. Conversely, a triangle can be made into a star, and the terminology "star-triangle transformation" is often used to refer to both of these operations.

Another probabilistic model known to possess a star-triangle transformation is the Ising model, a celebrated model of magnetization which samples a random config-

2020 Mathematics Subject Classification. Primary 82B20; Secondary 05C10, 05C62, 16T25.
Keywords. Star-triangle, Y-delta, Yang–Baxter equations, cube flips, cube moves, s-embedding, Ising model, embedding, harmonic embedding, integrable system.

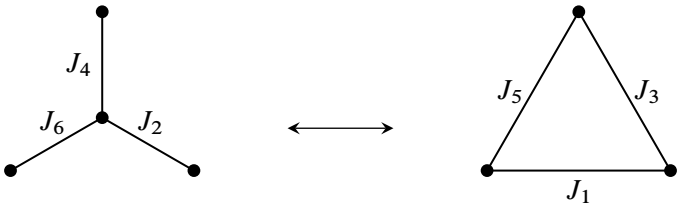

Figure 1. Star-triangle transformation.

uration of spins living at the vertices of a graph; this property appears in [26, 28], see also [3, Chapter 6]. The probability distribution of this configuration depends on coupling constants attached to the edges of the graph. When these coupling constants are all positive (which is called the ferromagnetic regime), one can perform a local transformation of the graph as in Figure 1 without changing the correlations of spins outside of the location where the transformation is performed [26,28]. Note, however, that the formulas relating the coupling constants before and after the transformation are not the same as those for the conductances in resistor networks.

Let G be a planar graph, that is, a graph that can be embedded in the plane or, equivalently, in the sphere. We denote by $G^\diamond$ its diamond graph, whose vertex set is composed of the vertices and dual vertices of G and whose faces are all quadrilaterals, one for each edge of G (see Figure 2). We note that planar graphs are graphs that can be embedded in the plane but which do not come with a distinguished embedding. From now on we will assume that every planar graph G is 3-connected, which implies [29] that it possesses a unique embedding up to homeomorphisms of the sphere. In particular, the faces of G are well-defined. Hence its diamond graph $G^\diamond$ is well-defined, is also 3-connected and has well-defined faces.

To each of the two models described above (random walk and Ising model) is associated a class of graph embeddings. More precisely, if G denotes a planar graph

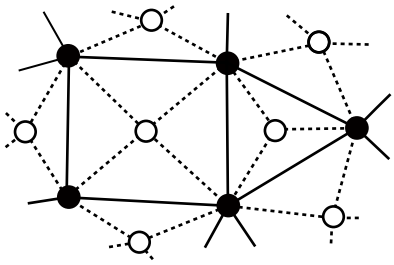

Figure 2. A piece of a planar graph G (black dots and solid lines), its dual vertices (white dots) and its diamond graph $G^\diamond$ (dotted lines).

carrying positive edge weights (conductances for the random walk, coupling constants for the Ising model), one embeds in the plane its diamond graph $G^\diamond$.

The embeddings associated to random walks are called the Tutte embeddings or harmonic embeddings [27] and have the property that the faces of $G^\diamond$ are embedded as orthodiagonal quads, that is, their diagonals are perpendicular. The conductance of an edge of G corresponding to an orthodiagonal quad embedding of a face of $G^\diamond$ is given by a ratio of the lengths of the diagonals of the quad. The embeddings associated to the ferromagnetic Ising model were introduced by Chelkak [6,7] under the name of s-embeddings; in this case the faces of $G^\diamond$ are embedded as tangential quads, which are quads admitting a circle tangential to the four sides. The coupling constant of an edge e of G corresponding to a tangential quad embedding of a face of $G^\diamond$ is given by

$$J_e = \frac{1}{2} \ln \Big(\frac{1 + \sin \theta_e}{\cos \theta_e} \Big),$$

where

$$\tan^2 \theta_e = \frac{\operatorname{cotan} \delta + \operatorname{cotan} \beta}{\operatorname{cotan} \alpha + \operatorname{cotan} \gamma},$$

and α, β, γ, δ denote the half-angles of the tangential quad, as shown in Figure 3. In the special case when the tangential quad is a rhombus, the angle θ_e arises as the half-angle of a corner of the quad corresponding to a primal vertex. In the general case, θ_e does not seem to have a geometric realization as an angle.

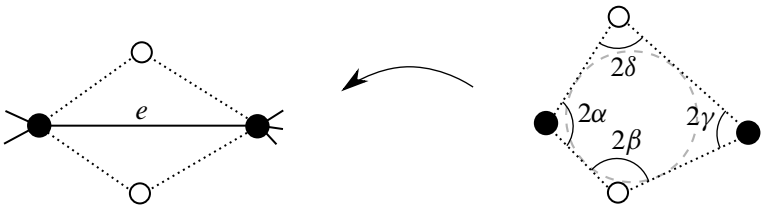

Figure 3. Relation between an abstract weighted graph and an s-embedding.

Existence and uniqueness questions for both harmonic embeddings and s-embeddings may be asked either for finite weighted graphs or infinite weighted graphs periodic in two directions. Complete answers are known for harmonic embeddings in both cases and for s-embeddings in the periodic case, see [6, 18] for a discussion. However, such questions are not relevant for our purposes, as we will start from one given embedding and discuss whether or not there exists another embedding related by a local transformation.

To avoid unnecessary complications related to boundary issues in the case of finite graphs, we will always assume that the edges involved in our star-triangle transformations are not boundary edges. Note that one could consider a broader framework

including such boundary edges, provided that one replaces the notion of a dual graph by that of the augmented dual graph, which has several dual vertices associated with the outer face, one between each pair of consecutive boundary vertices, see, e.g., [18].

A harmonic embedding or an s-embedding of the diamond graph $G^\diamond$ determines a drawing of G, since the vertices of G form a subset of the vertices of $G^\diamond$. However, a drawing of G does not uniquely determine a harmonic embedding or an s-embedding.

Such embeddings provide the appropriate geometric setting to observe conformally invariant objects such as Brownian motion or SLE processes when taking the scaling limits of random walks and Ising models on generic planar graphs [4, 6, 7]. They generalize isoradial embeddings (embeddings of the faces of $G^\diamond$ as rhombi), for which specific techniques can lead to proofs of scaling limits (for instance in [5, 8, 9, 12, 17] and others), but which correspond to specific choices of weights on an already embedded graph.

The star-triangle move for random walks (resp. the Ising model) translates into a geometric local move for harmonic embeddings (resp. for s-embeddings), whereby three orthodiagonal quads (resp. tangential quads) sharing a vertex as on the left-hand side picture of Figure 4 get erased and replaced by three other orthodiagonal quads (resp. tangential quads) with the same hexagonal outer boundary, as on the right-hand side picture of Figure 4. We call this geometric local move a *cube move*, phrase which was originally introduced in [19] only with a combinatorial meaning (and not a geometric one). We emphasize that cube moves for us are geometric local moves which apply to tilings of the plane by quads, while star-triangle transformations are combinatorial local moves which apply to graphs with edge weights.

The existence and uniqueness of the cube move for harmonic embeddings follows from a classical theorem of planar geometry called Steiner's theorem [18, 21]. In this article, we show the existence and uniqueness of the cube move for s-embeddings (see definitions in Section 2 and Theorem 3.1 for the exact statement).

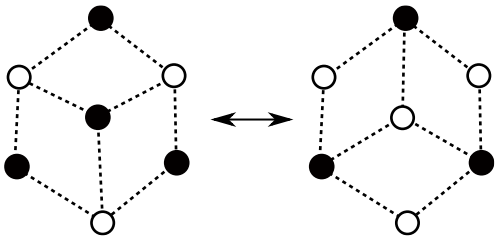

Figure 4. The transformation on $G^\diamond$ induced by the star-triangle transformation on G: a *cube move*.

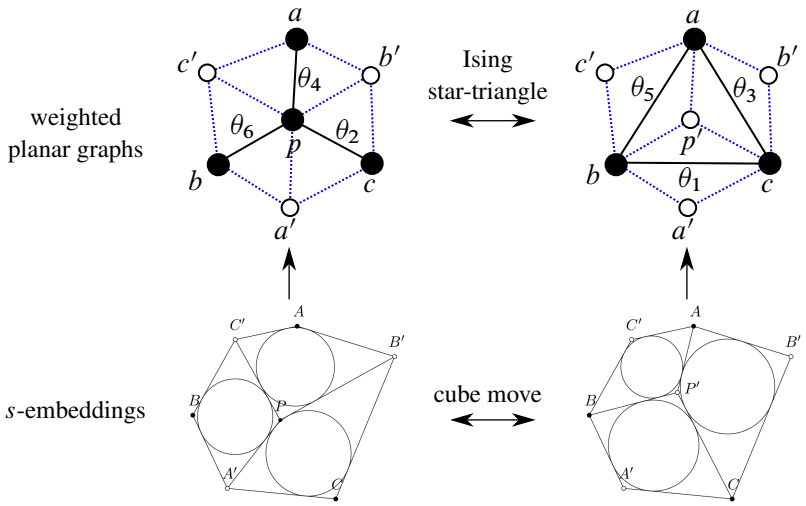

Figure 5. The star-triangle transformation for the Ising model is conjugated to a local geometric transformation called a *cube move*, via Chelkak's s-embeddings introduced in [6,7]. Notice that in the embedded graphs, only the central points P and P' differ.

Theorem 1.1. *For any s-embedding with the combinatorics of the graph on the left-hand side of Figure 4, erase the central black point and keep all the other points fixed. Then there exists a unique central white point that gives an s-embedding with the combinatorics of the graph on the right-hand side of Figure 4.*

Moreover, it follows from the construction in Section 3 of the s-embedding after the cube move that the coupling constants associated with this new s-embedding are the same as those obtained by applying the star-triangle transformation to the coupling constants associated with the s-embedding before the cube move. In other words, the star-triangle transformation of the Ising model only has a local effect on s-embeddings. This is illustrated by a commutative diagram in Figure 5. Our proof of existence relies only on [7, Proposition 4.7] by Chelkak, which connects a linear system on the graph (called *propagation equations*) to the construction of s-embeddings. We prove uniqueness via self-contained geometric arguments (see Section 3).

In passing, we prove new and simpler formulas for the transformation of coupling constants under the Ising star-triangle transformation.

Theorem 1.2. *Denote by J_2, J_4, J_6 (resp. J_1, J_3, J_5) the coupling constants before (resp. after) the star-triangle transformation for the Ising model, as in Figure 1. For every $1 \leq i \leq 6$, let θ_i be the unique angle in $(0, \frac{\pi}{2})$ such that*

$$J_i = \frac{1}{2} \ln \Big(\frac{1 + \sin \theta_i}{\cos \theta_i} \Big).$$

Then

$$\forall i \in \{2,4,6\},\ \cos(\theta_i) = \frac{\sin\theta_{i+3}\cos\theta_{i+1}\cos\theta_{i+5}}{\sin\theta_{i+3}+\sin\theta_{i+1}\sin\theta_{i+5}}, \tag{1.1}$$

$$\forall i \in \{1,3,5\},\ \sin(\theta_i) = \frac{\cos\theta_{i+3}\sin\theta_{i+1}\sin\theta_{i+5}}{\cos\theta_{i+3}+\cos\theta_{i+1}\cos\theta_{i+5}}, \tag{1.2}$$

where the indices are considered modulo 6.

Formulas (1.1) and (1.2) are considerably less involved than the classical transformation procedure which is described in Proposition 3.9. We stress that the relation between the coupling constants before and after the star-triangle transformation is the same as in [3, 26, 28]; what is new is the simpler expression for that relation.

In addition to the results on local transformations for s-embeddings and the Ising model presented above, the second main contribution of this article involves a new class of embeddings, called α-embeddings, which we introduce as a one-parameter common generalization of harmonic embeddings and s-embeddings. Given $\alpha \in \mathbb{R}^*$, we call a quadrilateral $ABCD$ drawn on the plane an *α-quad* if its side lengths satisfy $AB^\alpha + CD^\alpha = AD^\alpha + BC^\alpha$. The quadrilateral $ABCD$ may be non-convex or even have its edges intersecting away from their endpoints. An *α-embedding* of a graph G is an embedding of its diamond graph $G^\diamond$ such that each face of $G^\diamond$ is drawn as an α-quad. This definition is, firstly, motivated by the introduction of a unified framework for properties of harmonic and s-embeddings, which correspond to the cases $\alpha = 2$ and $\alpha = 1$, respectively. Secondly, the celebrated isoradial embeddings are α-embeddings for every α, since rhombi are α-quads for every α. More generally, kite embeddings are α-embeddings for every α, see Section 5. Thirdly, as we shall see, there is a whole range of parameters for which these quadrilaterals satisfy a version of a cube move. This property suggests the presence of an integrable system, and it would be remarkable to find a family of such systems indexed by a continuous parameter.

To state this version of the cube move, we introduce the weaker notion of an α-realization of G as a map from the vertices of $G^\diamond$ to the plane such that each face of $G^\diamond$ is mapped to an α-quad, with edges possibly intersecting. We also provide a definition of the above notions in the cases where $\alpha \in \{-\infty, 0, +\infty\}$. In addition, we show that, for $\alpha > 1$, the cube move is possible for α-realizations (although the solution may not be unique). See Theorem 4.7 for a precise statement.

Theorem 1.3. *Let $\alpha > 1$ be a real number. For any α-realization with the combinatorics of the graph on the left-hand side of Figure 4, erase the central black point and keep all the other points fixed. Then there exists a central white point that gives an α-realization with the combinatorics of the graph on the right-hand side of Figure 4.*

One may wonder whether a probabilistic model can be associated to α-embeddings beyond the cases where α is 1 or 2. In other words, is there a way to define the interaction constants of a probabilistic model from the local geometry of α-embeddings in such a way that the cube move for α-embeddings is conjugated to the star-triangle move for the probabilistic model? The FK-percolation model is a common generalization of the Ising model and of spanning trees (which have the same star-triangle transformation as random walks). This model also has a star-triangle transformation; however, it can be applied only when the weights satisfy some local constraint [11, 17], whereas the star-triangle transformation for the Ising model and spanning trees holds without any condition on the weights. We did not succeed in relating α-embeddings to FK-percolation for arbitrary weights that would satisfy the local constraint and do not expect such a general connection to hold true. Nevertheless, there exists a subclass of weights among those satisfying the local constraint which can be associated to isoradial embeddings, that is, embeddings where the quadrilaterals are rhombi. In that case, the star-triangle transformation corresponds to a cube move for rhombus tilings, which exists and is unique.

Organization of the paper. We define in Section 2 our main object of interest, α-quads; we introduce α-embeddings and α-realizations, before defining their cube move. Section 3 is devoted to the specific case $\alpha = 1$, where we recall the connection with the Ising model and prove the existence and uniqueness of the cube move for properly embedded graphs. We also prove Theorem 1.2. In Section 4, we show that for $\alpha > 1$, such a move is always possible under weaker conditions, which leads to the proof of Theorem 1.3. Finally, in Section 5, we investigate some more basic geometric properties of α-quads and we propose a general framework to study a broader class of quadrilaterals. Appendix A contains a brief introduction to Jacobi elliptic functions, which are one of our main tools in the proofs of Section 3.

2. Definitions

This section is devoted to the definition of the so-called α-quads—which are the main object of interest of this paper—of their embeddings and of their realizations. We introduce an operation on them called a *cube move*, before defining an important tool to prove this property, which we call *construction curves*.

In what follows, we denote by $\mathbb{R}^*$ the set $\mathbb{R} \setminus \{0\}$ and by $\overline{\mathbb{R}}$ the set $\mathbb{R} \cup \{-\infty, +\infty\}$ of extended real numbers. For two points A, B in the plane, AB denotes the Euclidean distance between A and B, and we use a dot to write products of lengths such as $AB.CD$.

2.1. α-embeddings and realizations

Let us start by defining the notion of α-quads.

Definition 2.1. A quadrilateral $ABCD$ is called an *α-quad* for $\alpha \in \mathbb{R}^*$ if

$$AB^\alpha + CD^\alpha = AD^\alpha + BC^\alpha.$$

It is called a 0-quad if

$$AB.CD = AD.BC,$$

a $+\infty$-quad if

$$\max(AB, CD) = \max(AD, BC)$$

and a $-\infty$-quad if

$$\min(AB, CD) = \min(AD, BC).$$

Note that the α-quads are not required to be convex nor even proper (see Definition 2.2), meaning that edges may intersect away from their endpoints.

One can immediately notice that α-quads (for $\alpha \in \overline{\mathbb{R}}$) are simply quadrilaterals $ABCD$ such that $f_\alpha(AB, CD) = f_\alpha(AD, BC)$, where for $x, y > 0$ we set $f_\alpha(x, y) = x^\alpha + y^\alpha$ if $\alpha \in \mathbb{R}^*$, $f_0(x, y) = xy$, $f_{+\infty}(x, y) = \max(x, y)$ and $f_{-\infty}(x, y) = \min(x, y)$. Such a notation calls for a generalization from f_α to any homogeneous symmetric function f of two variables, which is done at the end of Section 5.

Of particular interest are the following three families of α-quads, which were already defined in a different context:

- 1-quads correspond to *tangential quads*, i.e., quads such that there is a circle tangential to their four sides (see, e.g., [13]);
- 2-quads correspond to *orthodiagonal quads*, i.e., quads whose diagonals are perpendicular (see, e.g., [14]);
- 0-quads are known under the name of *balanced quads* [13] and contain a well-studied class of quads, the *harmonic quads*, which are defined as cyclic 0-quads (that is, 0-quads inscribed in a circle, see [2] for details).

Definition 2.2. For $n \geq 3$, an n-tuple of distinct points $A_1, \dots, A_n$ is said to be a *proper* polygon if the line segments $[A_1A_2], [A_2A_3], \dots, [A_{n-1}A_n], [A_nA_1]$ do not intersect except possibly at their endpoints. In other words, the closed piecewise linear curve $A_1, A_2, \dots, A_n, A_1$ is a Jordan curve.

A proper polygon is said to be *positively* (resp. *negatively*) *oriented* if the points on its boundary oriented counterclockwise (resp. clockwise) are $A_1, A_2, \dots, A_n$ in this order.

Let G be a planar graph, finite or infinite. Denote its dual graph by G^*, whose vertices are faces of G and where we connect two dual vertices if the two corresponding faces share an edge. We construct the graph $G^\diamond$ as the bipartite graph whose black (resp. white) vertices are the vertices of G (resp. G^*) and where an edge connects a black vertex to a white vertex whenever the black vertex is on the boundary of the face associated with the white vertex. In particular, all the faces of $G^\diamond$ are quadrilaterals, see Figure 2.

Definition 2.3. Let $\alpha \in \overline{\mathbb{R}}$. An *$\alpha$-embedding* of G is an embedding of $G^\diamond$ in the plane such that every internal face of $G^\diamond$ is an α-quad.

The fact that $G^\diamond$ is embedded in the plane implies that the α-quads corresponding to internal faces are proper. In particular, for embedded graphs, edges cannot collapse to a point, two distinct edges cannot meet outside of their endpoints, faces have non-empty interiors and two distinct faces have disjoint interiors. This setting is the one preferred for the study of statistical mechanical models such as spanning trees and the Ising model. However, in the more general setting we consider, we need to allow drawings of graphs that are not necessarily embeddings.

Definition 2.4. Let $\alpha \in \overline{\mathbb{R}}$. An *$\alpha$-realization* of G is defined to be any map from the vertices of $G^\diamond$ to the plane such that every face of $G^\diamond$ is mapped to an α-quad.

See Figure 7 for an example of a 4-embedding and a 4-realization of the same graph.

As mentioned in the introduction, there are two notable classes of examples of α-embeddings. The class of 1-embeddings of a planar graph corresponds to the class of s-embeddings defined by Chelkak in [6, 7] (see also [24]), while the class of 2-embeddings corresponds to the class of harmonic embeddings [18, 27].

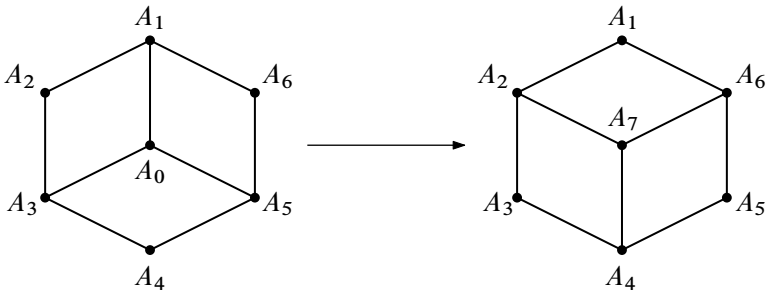

Figure 6. The combinatorics of a cube move for α-embeddings and α-realizations.

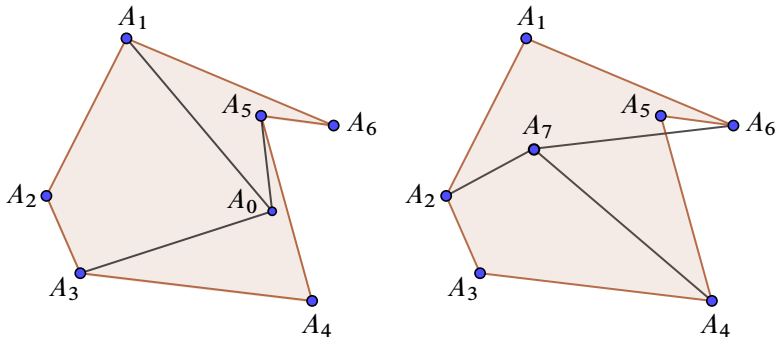

Figure 7. Here $\alpha = 4$. Left: an α-embedding of the portion of the graph on the left-hand side of Figure 6. Right: an α-realization of the portion of the graph on the right-hand side of Figure 6. The quad $A_4A_5A_6A_7$ on the right is not proper.

2.2. The cube move: setting

We now define the property that we want to study on α-quads, which we call the *flip property*. This property states that it is possible to perform a *cube move* like that of Figure 6 locally on the realization or embedding, while keeping the global structure unchanged.

Definition 2.5. For any $\alpha \in \overline{\mathbb{R}}$, the set of all α-realizations is said to satisfy the *flip property* if, for any six distinct points in the plane $A_1, A_2, \dots, A_6$ such that A_1, A_3, A_5 (resp. A_2, A_4, A_6) are not aligned, the following are equivalent:

- there exists a point A_0 such that $A_0, A_1, \dots, A_6$ is an α-realization of the graph on the left-hand side of Figure 6;
- there exists a point A_7 such that $A_1, \dots, A_7$ is an α-realization of the graph on the right-hand side of Figure 6.

The set of α-embeddings is said to satisfy the *proper flip property* if, in the equivalence of Definition 2.5, it is also required that the figures are α-embeddings, and that each of the quadrilaterals is proper, with its boundary vertices oriented in the same order as in Figure 6.

In both cases, it is said to satisfy the *unique* (proper) flip property if it satisfies the (proper) flip property and if, in addition, when the points A_0 and A_7 exist they are unique.

Our ultimate goal is to understand for which values of α these properties are satisfied by the set of α-realizations or α-embeddings. In this direction, we notably prove Theorem 3.1 for 1-embeddings and Theorem 4.7 for α-realizations with $\alpha > 1$, and conjecture a generalization to other values of α (see Conjecture 3.2). Note that it is

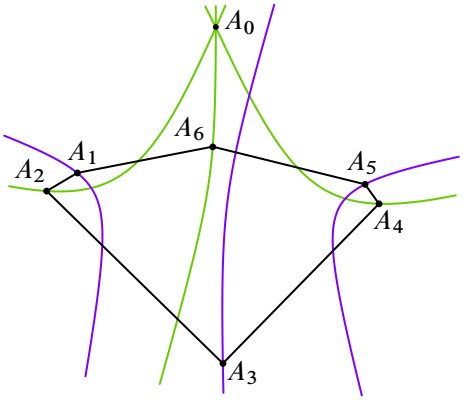

Figure 8. A configuration for $\alpha = 1$, with the corresponding construction curves. The green construction curves have an intersection point A_0 but the purple ones do not intersect.

already known that the set of 2-embeddings satisfies the unique proper flip property and that the set of 2-realizations satisfies the unique flip property. This can be proved using a theorem of Steiner, see [18, 21].

There is a necessary condition on the outer hexagon $A_1 \dots A_6$ in order to be in a position to flip three quads.

Proposition 2.6. *Let $A_1, \dots, A_6$ be six distinct points and let $\alpha \in \mathbb{R}$. Suppose that there is either a point A_0 producing an α-realization of the left-hand side of Figure 6 or a point A_7 producing an α-realization of the right-hand side of Figure 6. Then the side lengths of the hexagon $A_1 \dots A_6$ must satisfy*

$$A_1A_2^\alpha + A_3A_4^\alpha + A_5A_6^\alpha = A_2A_3^\alpha + A_4A_5^\alpha + A_6A_1^\alpha \quad \text{if } \alpha \neq 0, \tag{2.1}$$

$$A_1A_2.A_3A_4.A_5A_6 = A_2A_3.A_4A_5.A_6A_1 \quad \text{if } \alpha = 0. \tag{2.2}$$

Proof. When $\alpha \neq 0$, formula (2.1) follows immediately from summing the three equations defining the three α-quads involving A_0 (resp. A_7). The case $\alpha = 0$ works similarly. ∎

The example on Figure 8 with $\alpha = 1$ illustrates the fact that condition (2.1) is not sufficient to have an α-realization. Indeed, the existence of a point A_0 implies that condition (2.1) is satisfied, but there exists no point A_7. We also point out that there is no analogue of Proposition 2.6 when $\alpha = \pm\infty$.

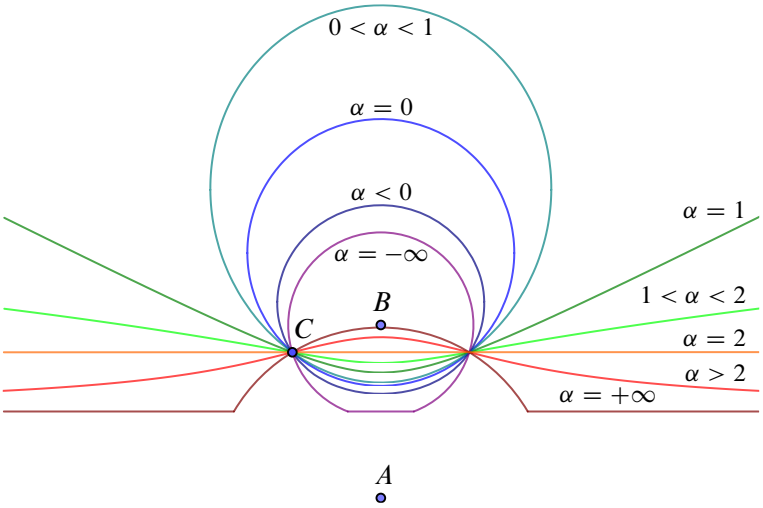

Figure 9. Construction curves with foci A and B going through C. The fact that they intersect only at C and at its symmetric with respect to (AB) is a consequence of Proposition 5.4. The asymptotic behavior of construction curves is described in Lemma 4.6.

2.3. Construction curves

In order to check the existence of the points A_0 and A_7 introduced in Definition 2.5, we will see them as intersection points of certain curves called construction curves. Let us first define them properly.

Definition 2.7. Let A, B and C be three distinct points in the plane and let $\alpha \in \overline{\mathbb{R}}$. The *$\alpha$-construction curve* with foci A, B going through C is the set of points M such that $ACBM$ is an α-quad.

Let $A_1, \dots, A_6$ be the distinct vertices of a hexagon. The α-construction curves of the hexagon $A_1 \dots A_6$ are the six curves $\mathcal{C}_i$ where for every $1 \leq i \leq 6$, $\mathcal{C}_i$ is defined to be the α-construction curve with foci A_{i-1} and A_{i+1} going through A_i. Here indices are taken modulo 6.

The role of construction curves in our problem is the following. Start with a hexagon $A_1A_2A_3A_4A_5A_6$ and let $\alpha \in \overline{\mathbb{R}}$. The existence of a point A_0 as on the left-hand side of Figure 6 is equivalent to the fact that $\mathcal{C}_2$, $\mathcal{C}_4$ and $\mathcal{C}_6$ have a common point, see Figure 10. Similarly the existence of a point A_7 as on the right-hand side of Figure 6 is equivalent to the fact that $\mathcal{C}_1$, $\mathcal{C}_3$ and $\mathcal{C}_5$ have a common point.

Remark 2.8. In order for the flip property to be satisfied when $\alpha \in \mathbb{R}$, it is actually enough to consider the intersection of two construction curves rather than three. Indeed, if $\alpha \neq 0$ and if $A_0, A_1, \dots, A_6$ are seven points such that the quadrilater-

als $A_1A_2A_3A_0$, $A_3A_4A_5A_0$ and $A_5A_6A_1A_0$ are all α-quads, then by Proposition 2.6 formula (2.1) is satisfied. Hence, if $\mathcal{C}_1$ and $\mathcal{C}_3$ have a common point A_7, then combining the equation of the two α-quads $A_2A_3A_4A_7$ and $A_6A_1A_2A_7$ with formula (2.1) yields that A_7 also lies on $\mathcal{C}_5$. The case $\alpha = 0$ works similarly, replacing formula (2.1) by formula (2.2).

In a few cases, the construction curves are well known. Fix two points A and B in the plane. If C is a point such that $AC = BC$, then clearly for any α the construction curve going through C is the perpendicular bisector of $[AB]$, which we denote from now on by $P(AB)$. Without loss of generality, we may assume in what follows that

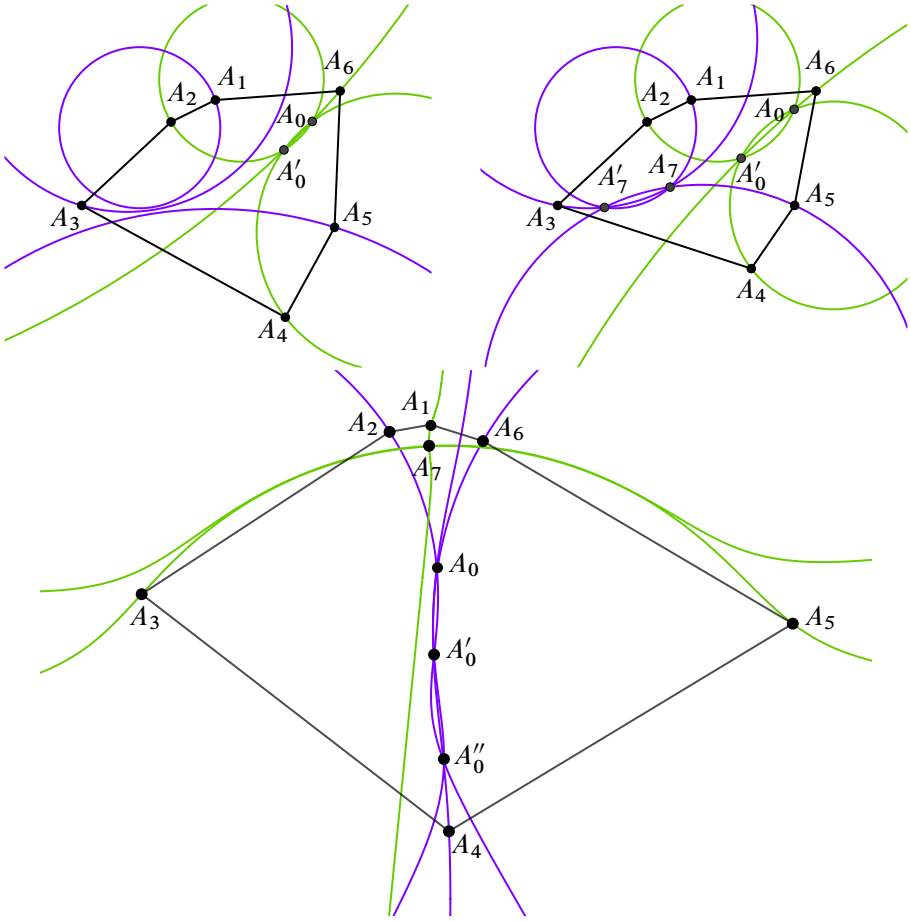

Figure 10. Examples of construction curves for some hexagons. Top left: for $\alpha = 0$, two possible points A_0 and no point A_7. Top right: for $\alpha = 0$, two points A_0 and two points A_7. Pictures with the same number of solutions as the top two pictures can be obtained for α close to 0. Bottom: for $\alpha = 10$, three points A_0 and one point A_7.

$BC < AC$. See Figure 9 for the general shape of construction curves depending on the value of α.

For any point O, we denote by $\mathcal{C}(O, C)$ the circle with center O going through C, and by $\mathcal{D}(O, C)$ the closed disk enclosed by $\mathcal{C}(O, C)$. The following proposition characterizes the construction curves in the special cases $\alpha \in \{-\infty, 0, 1, 2, +\infty\}$.

Proposition 2.9. *Let A, B and C be three points such that $BC < AC$. We denote by H the closed half-plane bounded by $P(AB)$ containing B. Then one has the following description for the α-construction curve with foci A, B going through C:*

- *For $\alpha = -\infty$, it is the union of the circular arc $\mathcal{C}(B, C) \cap H$ and the segment $P(A, B) \cap \mathcal{D}(B, C)$.*
- *For $\alpha = +\infty$, it is the union of the circular arc $\mathcal{C}(A, C) \cap H$ and the two half-lines $P(A, B) \cap \mathcal{D}(A, C)^c$.*
- *For $\alpha = 0$, it is a circle going through C.*
- *For $\alpha = 1$, it is the branch closest to B of the hyperbola with foci A, B going through C.*
- *For $\alpha = 2$, it is the perpendicular to (AB) going through C.*

Proof. For $\alpha = -\infty$, the curve is $\{M \in \mathbb{R}^2 \mid \min(AM, BC) = \min(BM, AC)\}$. The explicit description follows from a simple case handling, depending of the length realizing the minimum. The same goes for $\alpha = +\infty$.

For $\alpha = 0$, the curve is the set of points M such that the ratio $\frac{MA}{MB}$ is fixed, which is a circle by Apollonius's circle theorem.

For $\alpha = 1$, the curve is the set of points M such that $AM - BM$ is a fixed positive number, which is a branch of hyperbola with foci A, B.

For $\alpha = 2$, as stated in Section 5, the quadrilateral $ACBM$ is a 2-quad if and only if (AB) and (CM) are perpendicular. ∎

3. The cube move for $\alpha = 1$

Our goal in this section is to prove the unique proper flip property for 1-embeddings.

Theorem 3.1. *The set of 1-embeddings satisfies the unique proper flip property.*

Although our proof only works in this specific case, based on the observation of many numerical examples we expect the following more general result to hold.

Conjecture 3.2. *For any $\alpha \in [-\infty, 1]$ and for any six distinct points in the plane $A_1, A_2, \ldots, A_6$ such that A_1, A_3, A_5 (resp. A_2, A_4, A_6) are not aligned, the following are equivalent:*

- *there exists a* unique *point* A_0 *such that* $A_0, A_1, \dots, A_6$ *is an* α-embedding *of the graph on the left-hand side of Figure 6;*
- *there exists a* unique *point* A_7 *such that* $A_1, \dots, A_7$ *is an* α-embedding *of the graph on the right-hand side of Figure 6.*

Notice that this is weaker than the unique proper flip property, as it is possible that several points A_0 exist and no point A_7. Such a configuration is shown in the top-left picture of Figure 10. For the sake of completeness, let us also mention that the set of 1-realizations does not satisfy the flip property (when there is no "proper" requirement): there exist configurations such that there is a point A_0 yielding 1-realizations, but there is no point A_7 (see Figure 8).

The rest of this section is devoted to the proof of Theorem 3.1.

3.1. Uniqueness

In this first part, we prove the following proposition, which states the uniqueness of the point A_0, if it exists.

Proposition 3.3. *For any proper positively oriented hexagon* $A_1, A_2, \dots, A_6$*, there exists at most one point* A_0 *such that* $A_0, A_1, \dots, A_6$ *is a proper* 1*-embedding of the left-hand side of Figure 6.*

In order to prove it, we first need some information on the geometric properties of 1-quads. Notice that if three distinct points A, B, C are fixed, then the construction curve for 1-quads is the set of points D such that

$$AD - CD = AB - BC.$$

Hence, it is a hyperbola branch with foci A, C (with possible degenerate cases being the perpendicular bisector of $[AC]$, and half-lines $A + t(A - C)$ or $C + t(C - A)$ for $t \geq 0$). We put all these cases under the same name:

Definition 3.4. Let A, C be two distinct points in the plane. For any $\lambda \in \mathbb{R}$, the set of points D in the plane such that

$$AD - CD = \lambda \tag{3.1}$$

is called a *generalized hyperbola branch* with foci A and C.

The next lemma already implies that there are at most two admissible points A_0, in the sense of Proposition 3.3.

Lemma 3.5. *Assume that two generalized hyperbola branches have exactly one common focus, then they have at most two intersection points.*

Although this result, which appears in [25, 30], has a very classical flavor, we could not find any earlier reference. We give an alternative proof below.

Let us start with some definitions. The focus of a hyperbola branch $\mathcal{B}$ which belongs to (resp. does not belong to) the convex hull of $\mathcal{B}$ is said to be the *interior* (resp. *exterior*) focus of $\mathcal{B}$. For example, in Figure 11, A_1 is the interior focus of both branches while A_3 and A_5 are the exterior foci of these branches. Assume that $\mathcal{B}_1$ is a hyperbola branch with foci A and C and $\mathcal{B}_2$ is a hyperbola branch with foci A and E, with A, C, E distinct. Then any intersection point of $\mathcal{B}_1$ and $\mathcal{B}_2$ lies on a hyperbola branch $\mathcal{B}_3$ with foci C and E (whose equation is obtained by subtracting equation (3.1) for $\mathcal{B}_1$ and $\mathcal{B}_2$), and we can also suppose that $\mathcal{B}_3$ is not a line or a half-line. Then there is at least one of the three points A, C or E which is the interior focus of one branch and the exterior focus of another branch. Without loss of generality, we assume that A is the interior focus of $\mathcal{B}_1$ and the exterior focus of $\mathcal{B}_2$. We will show that these two branches intersect in at most two points.

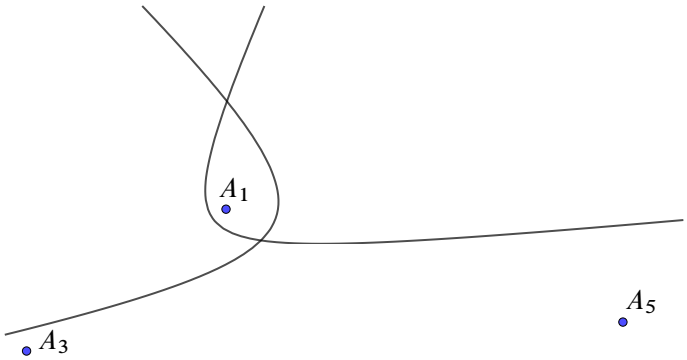

Figure 11. A case of two branches intersecting at two points. The focus A_1 is the interior focus of both branches.

Suppose that $\mathcal{B}_1$ and $\mathcal{B}_2$ intersect at three distinct points S, T, U. As these points belong to a non-degenerate hyperbola branch, they are not aligned. The lines (ST), (TU), (SU) therefore delimit exactly seven open regions in the plane, three of which touch the triangle STU only at one vertex. We call these three regions the *corner chambers* of S, T, U.

Lemma 3.6. *Let S, T and U be three distinct points on a hyperbola branch $\mathcal{B}$. Then the exterior focus of $\mathcal{B}$ belongs to a corner chamber of S, T, U, while the interior focus does not.*

Proof of Lemma 3.5. If one of the generalized branches is a line or a half-line, the result easily comes from the fact that a hyperbola and a line have at most two points of intersection.

Suppose now that it is not the case. The proof of Lemma 3.5 follows from Lemma 3.6, as A should be both in a corner chamber of S, T, U (because A is the exterior focus of $\mathcal{B}_2$) and not in one (because A is the interior focus of $\mathcal{B}_1$). ∎

Proof of Lemma 3.6. For any two distinct points A, B on $\mathcal{B}$, the line (AB) cuts the interior of the convex hull of $\mathcal{B}$ into a finite part and an infinite part. The half-plane delimited by (AB) that contains the finite part is called the *exterior half-plane* of A, B. It is easy to see that the exterior focus belongs to the exterior half-plane of A, B, for instance by noting that this property is invariant by affine transformations of the plane, and is straightforward to prove for the special branch $\{(x, y) \in (0, \infty)^2 \mid xy = 1\}$.

Suppose that T belongs to the exterior half-plane of S, U (which is equivalent to saying that S, T, U are met in that order when following the branch $\mathcal{B}$). Then, applying the previous property to (S, T) and (T, U), we get that the exterior focus has to belong to the corner chamber that touches T.

We now consider the interior focus of $\mathcal{B}$. By convexity of $\mathcal{B}$, the corner chambers are disjoint from the interior of the convex hull of $\mathcal{B}$, which by definition contains its interior focus. The result follows. ∎

We can now prove Proposition 3.3.

Proof of Proposition 3.3. By Lemma 3.5, there exists at most two such points. Suppose that there are two, A_0 and A_0'. We claim that A_1, A_3, A_5 belong to a unique hyperbola branch with foci A_0, A_0'. Indeed, since A_0, A_0' are on the same hyperbola branch with foci A_1, A_3, we have $A_1A_0 - A_3A_0 = A_1A_0' - A_3A_0'$. This is equivalent to $A_1A_0 - A_1A_0' = A_3A_0 - A_3A_0'$, which in turn means that A_1, A_3 are on the same hyperbola branch with foci A_0, A_0'. The same holds for A_5.

Therefore, by Lemma 3.6, one of the points A_0, A_0' is in a corner chamber of the triangle $A_1A_3A_5$, and the other is not. But notice that for any point M that does not belong to the lines (A_1A_3), (A_1A_5), (A_3A_5), the cyclic order of the vectors $\overrightarrow{MA_1}$, $\overrightarrow{MA_3}$, $\overrightarrow{MA_5}$ is always the same when M belongs to the union of the three corner chambers, and the opposite when M is outside that union. However, the cyclic order of the vectors $\overrightarrow{A_0A_1}$, $\overrightarrow{A_0A_3}$, $\overrightarrow{A_0A_5}$ should be the same as the cyclic order of the vectors $\overrightarrow{A_0'A_1}$, $\overrightarrow{A_0'A_3}$, $\overrightarrow{A_0'A_5}$, since this order should be fixed by the proper embedding. Therefore, it is impossible for both A_0 and A_0' to correspond to proper embeddings. ∎

3.2. Existence

The second part of this section consists in proving that, if we start with a proper 1-embedding $A_0, A_1, \ldots, A_6$ of the left-hand side of Figure 6, then there actually exists a point A_7 inducing a proper 1-embedding of the right-hand side. To show this,

we transform the problem into a linear one by using the *propagation equations* and *s-embeddings* defined by Chelkak [6,7]. We briefly explain this construction (we refer to Chelkak's original papers for more details), then give a few extra properties concerning the ordering of the vertices of the quads it gives, and finally apply it to our setting.

3.2.1. Ising model, propagation equations and *s*-embeddings. Let $G := (V, E)$ be a finite planar graph, in which each edge $e \in E$ carries a positive weight $J_e > 0$. The weights $(J_e)_{e\in E}$ are called the coupling constants of the ferromagnetic Ising model on G, that is, every spin configuration $\sigma \in \{\pm 1\}^V$ is assigned the Boltzmann weight

$$w(\sigma) = \exp\Big(\sum_{e=\{u,v\}\in E} J_e \sigma_u \sigma_v \Big),$$

and a spin configuration is randomly sampled with probability proportional to its Boltzmann weight. Note however that we will not refer to any statistical mechanical property of the Ising model thereafter; all the proofs are of purely geometric nature.

One checks that, for every $e \in E$ there exists a unique $\theta_e \in (0, \frac{\pi}{2})$ such that

$$J_e = \frac{1}{2} \ln \Big(\frac{1 + \sin \theta_e}{\cos \theta_e} \Big). \tag{3.2}$$

We also set

$$x_e = \tanh J_e = \tan \frac{\theta_e}{2} \in (0, 1). \tag{3.3}$$

Let G^c be the weighted graph whose vertices are the *corners* of the faces of G, and whose edges are of two types:

(1) those connecting two corners that correspond to the same vertex and to the same edge e of G; such edges carry the weight $\cos \theta_e$;

(2) those connecting two corners that correspond to the same face and to the same edge e of G; such edges carry the weight $\sin \theta_e$.

See Figure 12 for an illustration. There exists a double cover $\Upsilon^\times$ of G^c that branches around every edge, vertex and face of G, graphically represented around an edge in Figure 13 (see also Figure 17), which inherits the edge weights of G^c.

Let $V^\times$ be the vertices of $\Upsilon^\times$. We say that a function $X\colon V^\times \to \mathbb{C}$ satisfies the *propagation equation* if, for every $v \in V^\times$ with neighbours $v', v'' \in V^\times$ around an edge e like in Figure 13,

$$X_v = \sin \theta_e X_{v'} + \cos \theta_e X_{v''}.$$

It is easy to check that if X satisfies the propagation equation, its value is multiplied by -1 whenever we change sheets above a vertex of G^c.

If X is a solution to the propagation equation, then one can construct a function $\mathcal{S}\colon G^\diamond \to \mathbb{C}$, which is called the *s-embedding* associated to X, in the following way.

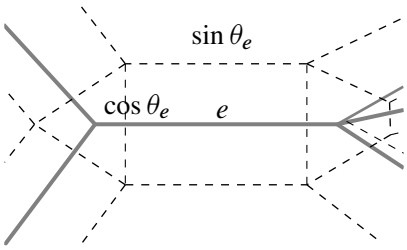

Figure 12. The corner graph G^c (dashed) around an edge e of G (solid).

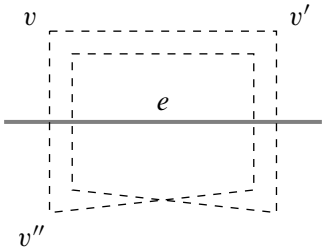

Figure 13. The double cover $\Upsilon^\times$ around the edge e of G.

Fix the image $\mathcal{S}(u_0)$ of a base vertex u_0 of G in the plane. Then define $\mathcal{S}$ such that for every vertex u of G and every face f adjacent to it, denoting by c the corner between u and f,

$$\mathcal{S}(f) - \mathcal{S}(u) = X_c^2, \tag{3.4}$$

where X_c is any of the two values of X above the corner c; both values produce the same constraint on $\mathcal{S}$. See Figure 14 for an example. Notice that it is not clear *a priori* that $\mathcal{S}$ is well-defined, as one needs to check at least that conditions (3.4) are closed around an edge, as in Figure 14. We will rely on the following result of Chelkak [7] that asserts that the s-embedding $\mathcal{S}$ is well-defined, and identifies s-embeddings with our notion of 1-embedding.

Proposition 3.7 ([7]). *For any solution X of the propagation equation such that $\mathrm{Re}(X)$, $\mathrm{Im}(X)$ are two vectors independent over $\mathbb{R}$, the associated s-embedding $\mathcal{S}$ is well-defined, and is such that every face of $G^\diamond$ is sent to a proper 1-quad in the complex plane. Conversely, for any 1-embedding $\mathcal{T}$ of G, for any edge $e \in E$ let θ_e be the unique angle in $(0, \frac{\pi}{2})$ such that, using the notation of Figure 3,*

$$\tan^2 \theta_e = \frac{\operatorname{cotan} \delta + \operatorname{cotan} \beta}{\operatorname{cotan} \alpha + \operatorname{cotan} \gamma}.$$

Then $\mathcal{T}$ is an s-embedding associated to a solution of the propagation equations on G with parameters $(\theta_e)_{e \in E}$.

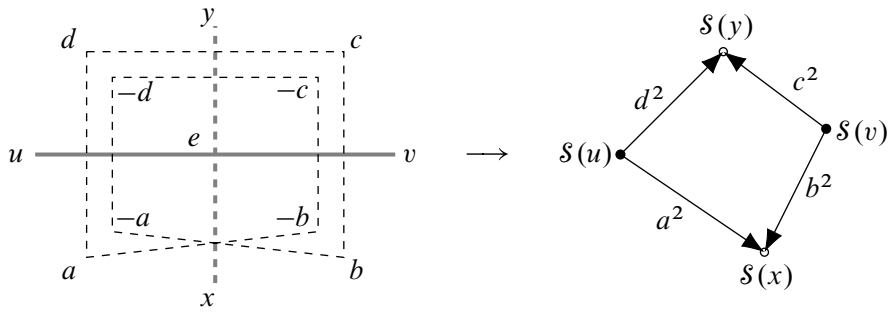

Figure 14. An edge $e \in E$ with vertices u, v and adjacent faces x, y, with a solution of its propagation equation, and the corresponding s-embedding, where the numbers $a^2, \dots, d^2$ are the complex coordinates of the vectors bounding the quad.

The plan of our proof of the existence part of the flip property is therefore to translate the initial configuration into a solution of the propagation equations, then show that one can apply a star-triangle transformation on this solution, and finally go back to embeddings. However, we need more information than what is contained in Proposition 3.7, as we want to keep track of the orientation of quadrilaterals. This is the aim of the following subsection.

3.2.2. Orientation of quads in s-embeddings.

Lemma 3.8. *Let $a, b, c, d \in \mathbb{C}^*$ be a solution to the propagation equation at an edge $e \in E$ with parameter $\theta \in (0, \frac{\pi}{2})$, set around e as in Figure 14. Suppose that $b/a \notin \mathbb{R}$. Then the following are equivalent:*

(i) *The 1-quad $\mathcal{S}(u)\mathcal{S}(x)\mathcal{S}(v)\mathcal{S}(y)$ is positively oriented.*

(ii) $\mathrm{Im}(b/a) > 0$.

(iii) *The cyclic order around the circle of the arguments of $\pm a$, $\pm b$, $\pm c$, $\pm d$ is $(a, d, c, b, -a, -d, -c, -b)$ (see Figure 15).*

Proof. The three statements are unaltered if we multiply all the complex numbers a, b, c, d by the same non-zero complex number. Hence we can suppose $a = 1$. Since the quad $\mathcal{S}(u)\mathcal{S}(x)\mathcal{S}(v)\mathcal{S}(y)$ is proper by Proposition 3.7, the sum of the representatives in $(0, 2\pi)$ of the oriented angles between pairs of vectors $\widehat{(a^2, d^2)}$, $\widehat{(b^2, a^2)}$, $\widehat{(c^2, b^2)}$, $\widehat{(d^2, c^2)}$ has to be either 2π if the quad is oriented positively or 6π if the quad is oriented negatively. In particular, the quad is oriented positively (resp. negatively) if and only if the arguments of a^2, d^2, c^2, b^2 (resp. b^2, c^2, d^2, a^2) are in that cyclic order around the circle.

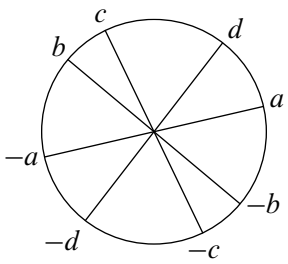

Figure 15. Cyclic order of the arguments of the complex numbers a, b, c, d.

- (iii) $\Rightarrow$ (i): Immediate consequence of the previous sentence.
- (ii) $\Rightarrow$ (iii): Suppose that $\mathrm{Im}(b) > 0$. Solving the propagation equation gives

$$c = \frac{b}{\cos\theta} + \tan\theta, \quad d = \frac{1}{\cos\theta} + b\tan\theta.$$

  Thus c and d are positive combinations of 1 and b, so their complex arguments lie between 0 and the argument of b. Moreover, one can compute:

$$\mathrm{Im}\left(\frac{c}{d}\right) = \frac{\cos^2\theta\,\mathrm{Im}(b)}{|1 + b\sin\theta|^2} > 0$$

  and we deduce that the order of the arguments matches the one of Figure 15.
- (i) $\Rightarrow$ (ii): Assume that (ii) is not verified, that is, $\mathrm{Im}(b) < 0$. Then consider $\overline{b}$, $\overline{c}$, $\overline{d}$, which is still a solution to the propagation equation as this equation has real coefficients. These values do satisfy (ii), hence also (iii) and thus (i) by the previous points. Note that they correspond to a quadrilateral that is the image by a reflection of our desired quad $\mathcal{S}(u)\mathcal{S}(x)\mathcal{S}(v)\mathcal{S}(y)$, and therefore for our initial solution (i) does not hold. ∎

3.2.3. Star-triangle transformation on propagation equations. This part consists in rephrasing Baxter's results on the star-triangle transformation of the Ising model (see [3, Section 6.4]). It is slightly easier to present it in the triangle-star direction, i.e., from the right-hand side to the left-hand side of Figure 16, although the converse is also possible.

Let us suppose that the graph G contains a triangle, as on the right-hand side of Figure 16. We label its edges with the parameters θ_i and define x_i, J_i as in (3.2) and (3.3). It is possible to transform the triangle into the star displayed on the left-hand side, while finding parameters such that both Ising models are coupled and agree everywhere except at A_7. This is called the *star-triangle transformation*.

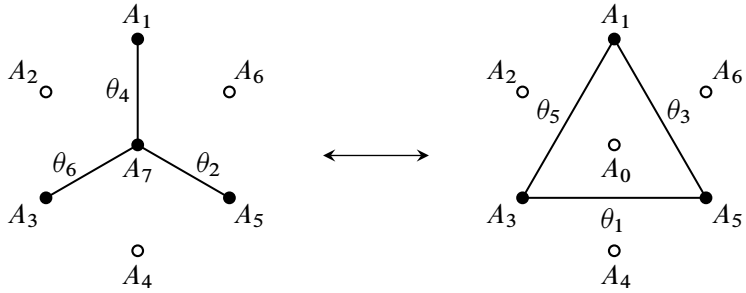

Figure 16. Star-triangle transformation on G (black vertices).

Proposition 3.9 ([3]). *Let $k' \in (0, \infty)$ be defined as*

$$k' = \frac{(1-x_1^2)(1-x_3^2)(1-x_5^2)}{4\sqrt{(1+x_1x_3x_5)(x_1+x_3x_5)(x_3+x_1x_5)(x_5+x_1x_3)}}.$$

Then the parameters θ_2, θ_4, θ_6 obtained by the star-triangle transformation are the unique angles in $(0, \frac{\pi}{2})$ such that

$$\forall i \in \{1,3,5\}, \quad \tan\theta_i \tan\theta_{i+3} = \frac{1}{k'}, \tag{3.5}$$

where the labels of the angles are considered modulo 6.

Remark 3.10. This transformation may be expressed in different ways; in this remark, we recall a convenient elliptic parametrization due to Baxter [3], also used in [5]. The previous definition of k' naturally comes from the use of an *elliptic modulus* $k \in i\mathbb{R} \cup [0,1)$ such that $k^2 + k'^2 = 1$; see Appendix A for a short introduction to elliptic functions.

We can define elliptic angles $\tau_1, \dots, \tau_6$ and $\theta'_1, \dots, \theta'_6$ by

$$\tau_i = \mathrm{F}(\theta_i, k), \quad \theta'_i = \frac{\pi\tau_i}{2\mathrm{K}(k)},$$

where F (resp. K) is the incomplete (resp. complete) integral of the first kind; see Appendix A for definitions and details. The normalization is such that both θ and θ' variables live in $(0, \frac{\pi}{2})$, while τ variables live in $(0, K(k))$. Then k can be seen as the only modulus such that the θ' angles satisfy

$$\theta'_1 + \theta'_3 + \theta'_5 = \frac{\pi}{2}. \tag{3.6}$$

In these parameters, the star-triangle transformation simply reads [3, 5]

$$\forall i \in \{1,3,5\}, \quad \theta'_{i+3} = \frac{\pi}{2} - \theta'_i. \tag{3.7}$$

We emphasize that this simple formula requires the introduction of a local elliptic modulus, while equations (1.1) and (1.2) do not.

The graphs $\Upsilon^\times$ corresponding to the star and to the triangle configurations are represented in Figure 17. We show that when the angles θ are chosen to satisfy the star-triangle relations (3.5), the propagation equations "seen from the boundary vertices" $w_1, \dots, w_6$ are the same.

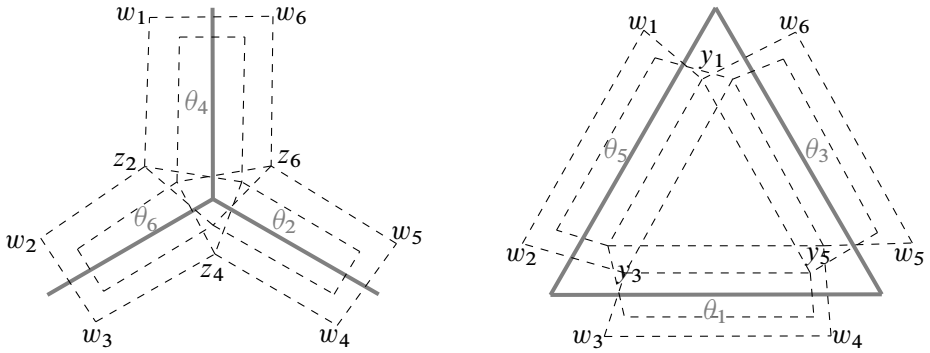

Figure 17. Star-triangle transformation of $\Upsilon^\times$.

Proposition 3.11. *Suppose that $\theta_1, \dots, \theta_6 \in (0, \frac{\pi}{2})$ satisfy the star-triangle relations (3.5). Let $(w_1, w_2, w_3, w_4, w_5, w_6, y_1, y_3, y_5)$ be a solution of the propagation equation on the "triangle" graph on the right of Figure 17. Then there exists a unique triple (z_2, z_4, z_6) such that $(w_1, w_2, w_3, w_4, w_5, w_6, z_2, z_4, z_6)$ is a solution of the propagation equation on the "star" graph on the left. Conversely, for any solution $(w_1, w_2, w_3, w_4, w_5, w_6, z_2, z_4, z_6)$ on the left, there exists a unique triple y_1, y_3, y_5 such that $(w_1, w_2, w_3, w_4, w_5, w_6, y_1, y_3, y_5)$ is a solution on the right.*

Proof. It is easy to see that any values of (y_1, y_3, y_5) uniquely characterize the solution of the propagation equation on the triangle graph. Thus, the set of possible vectors $(w_1, \dots, w_6)$ is a 3-dimensional subspace V. By setting (y_1, y_3, y_5) to be the elements of the canonical basis of $\mathbb{C}^3$ and solving the propagation equation, we get a basis of V:

$$u_1 = \begin{pmatrix} 1/\cos\theta_5 \\ \tan\theta_5 \\ 0 \\ 0 \\ \tan\theta_3 \\ 1/\cos\theta_3 \end{pmatrix}, \quad u_3 = \begin{pmatrix} \tan\theta_5 \\ 1/\cos\theta_5 \\ 1/\cos\theta_1 \\ \tan\theta_1 \\ 0 \\ 0 \end{pmatrix}, \quad u_5 = \begin{pmatrix} 0 \\ 0 \\ \tan\theta_1 \\ 1/\cos\theta_1 \\ 1/\cos\theta_3 \\ \tan\theta_3 \end{pmatrix}.$$

Similarly, the set of values of $(w_1, \dots, w_6)$ for the star graph is a subspace V' with basis

$$v_2 = \begin{pmatrix} 1/\sin\theta_4 \\ 1/\sin\theta_6 \\ 1/\tan\theta_6 \\ 0 \\ 0 \\ 1/\tan\theta_4 \end{pmatrix}, \quad v_4 = \begin{pmatrix} 0 \\ 1/\tan\theta_6 \\ 1/\sin\theta_6 \\ 1/\sin\theta_2 \\ 1/\tan\theta_2 \\ 0 \end{pmatrix}, \quad v_6 = \begin{pmatrix} 1/\tan\theta_4 \\ 0 \\ 0 \\ 1/\tan\theta_2 \\ 1/\sin\theta_2 \\ 1/\sin\theta_4 \end{pmatrix}.$$

We want to show that these subspaces are equal. By an argument of dimension, we just need to show that $v_2, v_4, v_6 \in V$. Let us do it for v_2, the other cases being symmetric. We claim that

$$\frac{1}{\cos\theta_3 \tan\theta_4} u_1 + \frac{1}{\cos\theta_1 \tan\theta_6} u_3 - \frac{\tan\theta_1}{\tan\theta_6} u_5 = v_2.$$

This is checked immediately for the third and fourth entries; the fifth and sixth entries are similar after noting that by (3.5),

$$\frac{\tan\theta_1}{\tan\theta_6} = \frac{\tan\theta_3}{\tan\theta_4}. \tag{3.8}$$

The first and second entries are a bit more tedious. For the first one, we want to show that

$$\frac{1}{\cos\theta_3 \tan\theta_4 \cos\theta_5} + \frac{\tan\theta_5}{\cos\theta_1 \tan\theta_6} = \frac{1}{\sin\theta_4}. \tag{3.9}$$

In terms of the elliptic variables $\tau_i = F(\theta_i, k)$ (see Appendix A), this amounts to showing (we omit the elliptic parameter k):

$$\mathrm{nc}(\tau_3)\,\mathrm{cs}(\tau_4)\,\mathrm{nc}(\tau_5) + \mathrm{nc}(\tau_1)\,\mathrm{sc}(\tau_5)\,\mathrm{cs}(\tau_6) - \mathrm{ns}(\tau_4) = 0. \tag{3.10}$$

By (3.7), $\tau_4 = \mathrm{K}(k) - \tau_1$ and $\tau_6 = \mathrm{K}(k) - \tau_3$, and by (3.6), $\tau_1 = \mathrm{K}(k) - (\tau_3 + \tau_5)$. Thus we can express all the arguments in terms of τ_3, τ_5. Using the change of arguments in elliptic functions (A.1), the left-hand side of (3.10) is equal to

$$\begin{aligned} &\mathrm{nc}(\tau_3)\,\mathrm{nc}(\tau_5)\,\mathrm{cs}(\tau_3+\tau_5) + \mathrm{sc}(\tau_3)\,\mathrm{sc}(\tau_5)\,\mathrm{ds}(\tau_3+\tau_5) - \mathrm{ns}(\tau_3+\tau_5) \\ &\quad = \mathrm{nc}(\tau_3)\,\mathrm{nc}(\tau_5)\,\mathrm{ns}(\tau_3+\tau_5) \\ &\qquad \times (\mathrm{cn}(\tau_3+\tau_5) + \mathrm{sn}(\tau_3)\,\mathrm{sn}(\tau_5)\,\mathrm{dn}(\tau_3+\tau_5) - \mathrm{cn}(\tau_3)\,\mathrm{cn}(\tau_5)). \end{aligned}$$

By (A.2), this is equal to zero.

For the second entry, we want to show that

$$\frac{\tan\theta_5}{\cos\theta_3 \tan\theta_4} + \frac{1}{\cos\theta_1 \tan\theta_6 \cos\theta_5} = \frac{1}{\sin\theta_6}. \tag{3.11}$$

By (3.5), we have that

$$\frac{\tan\theta_5}{\tan\theta_4} = \frac{\tan\theta_1}{\tan\theta_2}.$$

Hence (3.11) is equivalent to

$$\frac{\tan\theta_1}{\cos\theta_3\tan\theta_2} + \frac{1}{\cos\theta_1\tan\theta_6\cos\theta_5} = \frac{1}{\sin\theta_6}.$$

Up to a cyclic shift, this is the same as (3.9), so it holds by the previous discussion. ∎

As a byproduct of the previous proof, we obtain Theorem 1.2, which provides formulas expressing the change of θ parameters in the star-triangle transformation. These formulas are much simpler than the classical computation described in Proposition 3.9 and to the best of our knowledge, they are new.

Proof of Theorem 1.2. For $i = 4$, this follows from combining (3.8) and (3.9). Cyclic shifts of indices give the cases $i = 2$ and $i = 6$.

To obtain the other three values of i, we apply the Kramers–Wannier duality of the Ising model [22], which has the effect of transforming the variables θ_i into $\frac{\pi}{2} - \theta_i$. In this duality, the star graph becomes its dual, i.e., a triangle, and vice-versa. Hence the formula can be deduced from the previous one by changing sines into cosines and vice-versa. ∎

We now have all the elements to prove the unique proper flip property of 1-embeddings.

Proof of Theorem 3.1. We start with $A_0, A_1, \dots, A_6$, a proper embedding of the left-hand side of Figure 6. As uniqueness is a consequence of Proposition 3.3, we just have to prove that there exists a point A_7 such that $A_1, A_2, \dots, A_7$ is a proper embedding of the right-hand side.

By Proposition 3.7, there exists a solution $(w_1, w_2, w_3, w_4, w_5, w_6, y_1, y_3, y_5)$ of the propagation equation as on the left-hand side of Figure 17 such that the points $A_0, A_1, \dots, A_6$ are the s-embedding of this solution. Hence, by Proposition 3.11, there exists (z_2, z_4, z_6) such that $(w_1, w_2, w_3, w_4, w_5, w_6, z_2, z_4, z_6)$ is a solution to the propagation equation of the right-hand side of Figure 17. Let us consider its s-embedding. It has the same boundary as the initial one—hence the points $A_1, \dots, A_6$ are unchanged—and we have a new point A_7. It remains to prove that the three new 1-quads are proper and oriented as on the right-hand side of Figure 6. Then w_1/w_2 is not a real number. Indeed, if it were the case, the propagation equations would imply that the variables $(w_1, w_2, w_3, w_4, w_5, w_6, z_2, z_4, z_6)$ all have the same argument, and the initial embedding would not be proper. Moreover, the initial quad $A_1A_2A_3A_0$ is proper and positively oriented. Hence, we can apply Lemma 3.8 to obtain the ordering

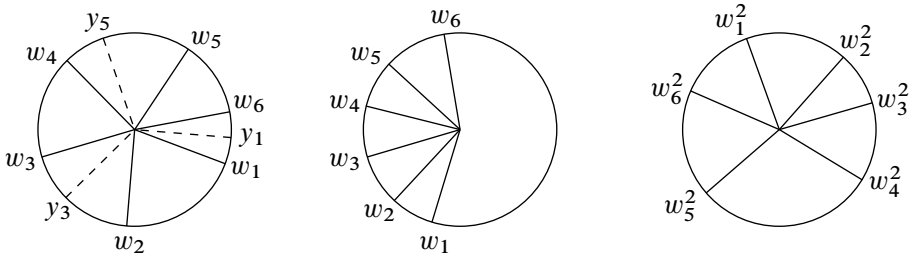

Figure 18. The cyclic order of the arguments of the variables w_i and y_i.

of the arguments of w_1, w_2, y_3, y_1. By doing the same for the other two initial quads, the order of the arguments of the variables w_i and y_i is that on the left of Figure 18.

Let us prove that the new (proper) quad $A_1A_2A_7A_6$ is positively oriented. By Lemma 3.8, it is enough to prove that $\mathrm{Im}(w_6/w_1) > 0$. If this is not the case, then we are in the situation of the second configuration of Figure 18, where all the arguments are included in a half-circle. Therefore we can get the order of the arguments of the w_i^2, as in the picture on the right of Figure 18. However, as in the proof of Lemma 3.8, the successive internal angles of the hexagon $A_1A_2A_3A_4A_5A_6$ can be expressed as the successive oriented angles in direct order in this last figure, and, in particular, their sum is 2π. This contradicts the fact that the hexagon is non-crossed, as the sum should be 4π. By symmetry, the three new quads are properly oriented, which concludes the proof. ∎

Remark 3.12. The so-called *exact bosonization* operation provides a map from two independent Ising models on some planar graph G to a bipartite dimer model on a modified graph $\widetilde{G}$ [10]. Under this correspondence, the Ising star-triangle move corresponds to the composition of six local moves for the dimer model called urban renewals [20, Figure 6]. On the other hand, embeddings as centers of circle patterns are known to be adapted to bipartite dimer models and the counterpart of urban renewal for these geometric objects is called the Miquel move [18]. From all this, we conclude that it is possible to write the star-triangle move for s-embeddings as a composition of six Miquel moves.

4. The cube move for $\alpha > 1$

In this section, we prove that the set of α-realizations for $\alpha > 1$ satisfies the flip property. In order to achieve this, we first study basic properties of construction curves, namely (un)boundedness, connectedness and asymptotic behaviour.

4.1. Properties of construction curves

Recall that construction curves for $\alpha \in \{-\infty, 0, 1, 2, +\infty\}$ are completely characterized by Proposition 2.9. In the rest of this section, we restrict ourselves to $\alpha \in \mathbb{R} \setminus \{0, 1, 2\}$.

Without loss of generality, to study an α-construction curve with foci A, B, we can assume that $A = (0, -1)$ and $B = (0, 1)$. Then any α-construction curve is characterized by a parameter $\lambda \in \mathbb{R}$, such that the curve is the set of points $\{M \in \mathbb{R}^2 \mid MA^\alpha - MB^\alpha = \lambda\}$. Hence, it is a level set of the function $F_\alpha : M \mapsto MA^\alpha - MB^\alpha$, or

$$F_\alpha(x, y) = (x^2 + (y+1)^2)^{\alpha/2} - (x^2 + (y-1)^2)^{\alpha/2}.$$

We denote this curve by $C(\alpha, \lambda) := F_\alpha^{-1}(\{\lambda\})$. Remark that when $\lambda = 0$ the curve $C(\alpha, 0)$ is $P(AB)$, which in that case is the horizontal axis. Moreover, changing λ into $-\lambda$ has the effect of reflecting the curve across $P(AB)$. Finally, note that the curve may be empty for some values of α and λ.

The following result is immediate.

Lemma 4.1. *Let M be a point distinct from A, B. Let M' be the image of M by the reflection across (AB), and M'' the image of M by the reflection across $P(AB)$. Then one has $F_\alpha(M) = F_\alpha(M') = -F_\alpha(M'')$. In particular, F_α is the zero function on $P(AB)$. Moreover, F_α has a constant sign on each half-plane bounded by $P(AB)$.*

Corollary 4.2. *For $\alpha \in \mathbb{R}^*$ and $\lambda > 0$, $C(\alpha, \lambda)$ is symmetric with respect to the axis (AB) and remains on one side of $P(AB)$ (namely, the side containing B if $\alpha > 0$ and the side containing A if $\alpha < 0$).*

In order to understand the level sets of the function F_α, let us study its profile. As a result of the symmetries of Lemma 4.1, it is sufficient to do so in the quadrant $(\mathbb{R}_+)^2$.

Lemma 4.3. *For any $M = (x_M, y_M) \in (\mathbb{R}_+)^2$,*

(i) *if $\alpha < 0$, then:*
- *F_α is C^∞ on $\mathbb{R}^2 \setminus \{A, B\}$;*
- *$\lim_{M \to B} F_\alpha(M) = -\infty$ and $\lim_{x_M^2 + y_M^2 \to \infty} F_\alpha(M) = 0$;*
- *$F_\alpha(M) < 0$ for $y_M > 0$ and $M \neq B$;*
- *$\frac{\partial F_\alpha}{\partial x}(M) > 0$ for $x_M > 0$ and $y_M > 0$;*
- *$\frac{\partial F_\alpha}{\partial y}(M) < 0$ for $x_M = 0$ and $y_M < 1$; $\frac{\partial F_\alpha}{\partial y}(M) > 0$ for $x_M = 0$ and $y_M > 1$;*

(ii) *if $0 < \alpha < 1$, then:*
- *F_α is continuous on $\mathbb{R}^2$, and C^∞ on $\mathbb{R}^2 \setminus \{A, B\}$;*
- *$\lim_{x_M^2 + y_M^2 \to \infty} F_\alpha(M) = 0$;*

- $F_\alpha(M) > 0$ *for* $y_M > 0$;
- $\frac{\partial F_\alpha}{\partial x}(M) < 0$ *for* $x_M > 0$ *and* $y_M > 0$;
- $\frac{\partial F_\alpha}{\partial y}(M) > 0$ *for* $x_M = 0$ *and* $y_M < 1$; $\frac{\partial F_\alpha}{\partial y}(M) < 0$ *for* $x_M = 0$ *and* $y_M > 1$;

(iii) *if* $\alpha > 1$ *with* $\alpha \neq 2$, *then:*

- F_α *is* C^1 *on* $\mathbb{R}^2$, *and* C^∞ *on* $\mathbb{R}^2 \setminus \{A, B\}$;
- $\lim_{y_M \to \infty} F_\alpha(M) = +\infty$ *for any fixed* $x_M \geq 0$;
- $F_\alpha(M) > 0$ *for* $y_M > 0$;
- $\frac{\partial F_\alpha}{\partial x}(M) < 0$ *for* $x_M > 0$, $y_M > 0$ *and* $\alpha < 2$; $\frac{\partial F_\alpha}{\partial x}(M) > 0$ *for* $x_M > 0$, $y_M > 0$ *and* $\alpha > 2$;
- $\frac{\partial F_\alpha}{\partial y}(M) > 0$ *for* $x_M, y_M \geq 0$.

Proof. Firstly, all the claims on the regularity of F_α are clear. Furthermore, the sign of this function on the quadrant $(\mathbb{R}_+)^2$ is apparent as well, since $MA \geq MB$ with equality only if $x_M = 0$.

Let us now deal with the asymptotic behaviour of F_α. For $\alpha < 0$, MB^α tends to $+\infty$ as $M \to B$ and therefore $\lim F_\alpha = -\infty$. On the other hand, for any $\alpha < 1$, notice that by the mean value theorem, for any M there exists a $u \in [MA, MB]$ such that

$$F_\alpha(M) = (MA - MB)\alpha u^{\alpha-1} \leq \alpha AB.MB^{\alpha-1},$$

where we used the triangular inequality. This tends to 0 as MB grows. In the case $\alpha > 1$, let x_M be fixed. For any large enough y_M, by the mean value theorem, there exists a $u \in [y_M - 1, y_M + 1]$ such that

$$F_\alpha(M) = u\alpha(x^2 + u^2)^{\alpha/2-1}.$$

For large y_M, this is equivalent to $\alpha y_M^{\alpha-1}$ and so it tends to $+\infty$.

We finally consider the partial derivatives of F_α. For any $M \in (\mathbb{R}_+^*)^2$, one can compute

$$\frac{\partial F_\alpha}{\partial x}(M) = \alpha x_M(MA^{\alpha-2} - MB^{\alpha-2}),$$

and its sign is apparent. Regarding the second partial derivative of F_α, we compute

$$\begin{aligned}\frac{\partial F_\alpha}{\partial y}(M) = {} & \alpha(y_M + 1)(x_M^2 + (y_M + 1)^2)^{\frac{\alpha}{2}-1} \\ & - \alpha(y_M - 1)(x_M^2 + (y_M - 1)^2)^{\frac{\alpha}{2}-1}. \end{aligned} \tag{4.1}$$

Let us investigate the case $\alpha < 1$. When $x_M = 0$ and $y_M \neq 1$, this reduces to

$$\alpha(\operatorname{sgn}(y_M + 1)|y_M + 1|^{\alpha-1} - \operatorname{sgn}(y_M - 1)|y_M - 1|^{\alpha-1}).$$

A study of the function $t \mapsto \operatorname{sgn}(t)|t|^{\alpha-1}$ shows that, for $\alpha \in (0,1)$, this quantity is positive when $y_M < 1$ and negative when $y_M > 1$ (and conversely for $\alpha < 0$).

Finally, we treat the case $\alpha > 1$. Using the expression (4.1), in order to prove that $\frac{\partial F_\alpha}{\partial y}(M) > 0$, we only have to prove that $g: u \to u(x_M^2 + u^2)^{\alpha/2-1}$ is increasing for any $x_M \geq 0$. For $x_M = 0$, the previous argument applies. For $x_M > 0$, g is differentiable and, for $u \in \mathbb{R}$, $g'(u) = [x_M^2 + (\alpha-1)u^2](x_M^2 + u^2)^{\alpha/2-2} > 0$. Hence, g is increasing and the result follows. ∎

The study of the function F_α allows one to prove that the curve $C(\alpha, \lambda)$ is obtained from the graph of a real function.

Corollary 4.4. *Let $\alpha \in \mathbb{R} \setminus \{0,1,2\}$ and $\lambda \in \mathbb{R}^*$. We assume that $\alpha\lambda > 0$, which ensures that the curve $C(\alpha,\lambda)$ is in the upper half-plane.*

For $\alpha < 1$, the curve $C(\alpha,\lambda)$ is bounded. If the curve is non-empty, there exists $0 < y_- < 1 < y_+$ such that $C(\alpha,\lambda) \cap (AB) = \{(0,y_-),(0,y_+)\}$. For any $y \in [y_-, y_+]$, there exists a unique $g_\alpha(y) \geq 0$ such that $(g_\alpha(y), y) \in C(\alpha,\lambda)$. Furthermore, the function g_α is C^1 on (y_-, y_+).

For $\alpha > 1$, the curve $C(\alpha,\lambda)$ is unbounded and, for any $x \in \mathbb{R}$, there exists a unique $f_\alpha(x) \in \mathbb{R}$ such that $(x, f_\alpha(x)) \in C(\alpha,\lambda)$. The function f_α is C^1 on $\mathbb{R}$. Moreover, for all $x \in \mathbb{R}$, $f_\alpha(x) > 0$, and on the interval $[0,\infty)$, the function f_α is increasing for $1 < \alpha < 2$, decreasing for $\alpha > 2$.

Proof. The (un)boundedness of the curve follows from the limits of Lemma 4.3, while the existence of g_α, f_α follows from the intermediate value theorem. In addition, by the implicit function theorem, all these functions are C^1. From the definition of the construction curve, we get that, for any $x \in \mathbb{R}$:

$$\frac{\partial F_\alpha}{\partial x}(x, f_\alpha(x)) + f'_\alpha(x)\frac{\partial F_\alpha}{\partial y}(x, f_\alpha(x)) = 0.$$

By Lemma 4.3, for all $x \in \mathbb{R}$, $\frac{\partial F_\alpha}{\partial x}(x, f_\alpha(x)) > 0$; moreover $\frac{\partial F_\alpha}{\partial y}(x, f_\alpha(x)) > 0$ if $\alpha > 2$ and $\frac{\partial F_\alpha}{\partial y}(x, f_\alpha(x)) < 0$ if $1 < \alpha < 2$. The result follows. ∎

Corollary 4.5. *$C(\alpha,\lambda)$ is a connected curve.*

Proof. By Lemma 4.3, for any $(x,y) \in \mathbb{R}^2$, $\frac{\partial F}{\partial y}(x,y) > 0$. We can therefore use the implicit function theorem along with Corollary 4.4 to get the result. ∎

We now investigate the asymptotic behaviour of the function f_α at $+\infty$ (and thus the asymptotic direction of the associated construction curve). The following lemma states that, in the case $1 < \alpha < 2$, the construction curve admits the perpendicular bisector of $[AB]$ as asymptotic direction, and in the case $\alpha > 2$, it is the actual asymptote of the curve.

Lemma 4.6. *Let $\alpha \in (1,\infty) \setminus \{2\}$, and $\lambda \neq 0$. As $|x| \to \infty$, $f_\alpha(x)$ has the following asymptotic behaviour:*

$$f_\alpha(x) \sim \frac{\lambda}{2\alpha}|x|^{2-\alpha}.$$

Proof. By the symmetry properties of $C(\alpha,\lambda)$, we only have to focus on the case $x \to +\infty$. For any $x > 0$, by the mean value theorem, there exists $u_x \in (f_\alpha(x)-1, f_\alpha(x)+1)$ such that

$$\begin{aligned}\lambda &= (x^2+(f_\alpha(x)+1)^2)^{\alpha/2} - (x^2+(f_\alpha(x)-1)^2)^{\alpha/2}\\ &= 2\alpha u_x (x^2+u_x^2)^{\alpha/2-1} = 2\alpha u_x^{\alpha-1}\Big(\frac{u_x}{x}\Big)^{2-\alpha}\Big(1+\Big(\frac{u_x}{x}\Big)^2\Big)^{\alpha/2-1}.\end{aligned}$$

For $1 < \alpha < 2$, this implies that $\frac{u_x}{x}$ tends to 0 as $x \to \infty$; otherwise the right-hand term would take arbitrarily large values. From this observation, we get that $u_x^{\alpha-1}(\frac{u_x}{x})^{2-\alpha} = \lambda(1+o(1))$ and therefore that $u_x \sim \frac{\lambda}{2\alpha}x^{2-\alpha}$. Since $u_x \in (f_\alpha(x)-1, f_\alpha(x)+1)$, the same holds for $f_\alpha(x)$.

For $\alpha > 2$, as $x \to \infty$, u_x has to converge to 0, and therefore $f_\alpha(x)$ is bounded. Asymptotically, as $x \to \infty$,

$$\begin{aligned}\lambda &= (x^2+(f_\alpha(x)+1)^2)^{\alpha/2} - (x^2+(f_\alpha(x)-1)^2)^{\alpha/2}\\ &\sim \frac{\alpha}{2}x^{\alpha-2}[(f_\alpha(x)+1)^2 - (f_\alpha(x)-1)^2] \sim 2\alpha f_\alpha(x)x^{\alpha-2},\end{aligned}$$

and the result follows. ∎

4.2. Flip property for $\alpha > 1$

We now go back to the study of the flip property of α-realizations. We get the following result in the case $\alpha > 1$:

Theorem 4.7. *For any real number $\alpha > 1$, the set of α-realizations satisfies the flip property.*

Proof. Fix $\alpha > 1$ and consider six distinct points $A_1, \dots, A_6$ such that A_1, A_3, A_5 (resp. A_2, A_4, A_6) are not aligned. Suppose that there is a point A_0 such that the quadrilaterals $A_1A_2A_3A_0$, $A_3A_4A_5A_0$ and $A_5A_6A_1A_0$ are all α-quads. By Remark 2.8, it suffices to show that the α-construction curves of the hexagon $\mathcal{C}_1$ and $\mathcal{C}_3$ have a common point. By Lemma 4.6, $\mathcal{C}_1$ admits $P(A_2A_6)$ as an asymptotic direction and $\mathcal{C}_3$ admits $P(A_2A_4)$ as an asymptotic direction. These two lines are not parallel, since A_2, A_4, A_6 are not aligned. Therefore, considering the behaviour of $\mathcal{C}_1$ and $\mathcal{C}_3$ at infinity and using Corollary 4.5, these two construction curves have to intersect at least once. ∎

Remark 4.8. It may be interesting to bound the number of intersection points of two construction curves having a focus in common, in order to control the number of potential points that could appear. Based on simulations, we expect that for $\alpha < 1$ there are at most two points of intersection, and for $\alpha > 1$ there are at most three (see the examples of Figure 10). It may be possible to use an analysis similar to that of Lemma 4.3 to get properties of convexity of the construction curves and deduce the previous bounds.

5. The space of α-quads and f-quadrilaterals

In this last section, we provide different geometric characterizations of α-quads. It appears that one of them holds in the broader context of f-quadrilaterals (see Definition 5.5). The first characterization of α-quads is related to the existence in the quadrilateral of a so-called *extremal pair*.

Definition 5.1. A pair of opposite sides of a quadrilateral is called an *extremal pair* if these two sides achieve both the maximum and the minimum of the side lengths of the quadrilateral.

Proposition 5.2. *A quadrilateral is an α-quad for some $\alpha \in \overline{\mathbb{R}}$ if and only if it has an extremal pair.*

Proof. Let Q be a quadrilateral whose side lengths are denoted by $\ell_1, \ell_2, \ell_3, \ell_4$ in cyclic order (starting from any of them). Assume that Q has no extremal pair. Then, without loss of generality, one may assume that ℓ_1 is the maximal length and ℓ_4 the minimal length, and they are distinct. Since (ℓ_1, ℓ_3) is not an extremal pair, ℓ_3 does not achieve the minimum. Thus, $\ell_3 > \ell_4$ and Q is not a $-\infty$-quad. Similarly, ℓ_2 does not achieve the maximum; thus, $\ell_2 < \ell_1$ and Q is not a $+\infty$-quad. By these inequalities, $\ell_1^\alpha + \ell_3^\alpha > \ell_2^\alpha + \ell_4^\alpha$ if $\alpha > 0$ and $\ell_1^\alpha + \ell_3^\alpha < \ell_2^\alpha + \ell_4^\alpha$ if $\alpha < 0$ (and in any of these cases Q is not an α-quad). Furthermore, $\ell_1\ell_3 > \ell_2\ell_4$ and Q is not a 0-quad. Hence, Q is not an α-quad for any $\alpha \in \overline{\mathbb{R}}$.

Conversely, suppose that Q has an extremal pair. We can assume that ℓ_1 is the maximal length, ℓ_3 the minimal length, and that $\ell_2 \leq \ell_4$ (up to a possible mirror symmetry). If $\ell_2 = \ell_3$ or if $\ell_4 = \ell_1$, then Q is a $-\infty$-quad or a $+\infty$-quad, respectively. Hence, we can assume that $\ell_3 < \ell_2 \leq \ell_4 < \ell_1$. Consider now the function g on $\mathbb{R}^*$ defined as

$$g\colon \alpha \mapsto \frac{\ell_1^\alpha + \ell_3^\alpha - \ell_2^\alpha - \ell_4^\alpha}{\alpha}.$$

The function g can be extended to a continuous function on $\mathbb{R}$ by setting $g(0) = \ln(\frac{\ell_1\ell_3}{\ell_2\ell_4})$. By the previous inequalities, for $\alpha \to -\infty$, $g(\alpha) \sim \frac{\ell_3^\alpha}{\alpha} < 0$ and for $\alpha \to +\infty$,

$g(\alpha) \sim \frac{\ell_1^\alpha}{\alpha} > 0$. Hence, by the intermediate value theorem, there exists $\alpha \in \mathbb{R}$ such that $g(\alpha) = 0$ and Q is an α-quad. ∎

We now characterize quadrilaterals that are α-quads for at least two distinct values of α.

Definition 5.3. A quadrilateral $ABCD$ is said to be a *kite* if its side lengths satisfy

$$\{AB, CD\} = \{BC, DA\}.$$

Remark, in particular, that a kite is an α-quad for all values of $\alpha \in \overline{R}$.

Proposition 5.4. *Let $\alpha \neq \alpha' \in \overline{\mathbb{R}}$, and let Q be a quad which is an α-quad and an α'-quad at the same time. Then Q is a kite.*

This generalizes a result of [13] which claims that a quad which is both a 0-quad and a 1-quad is a kite.

Proof. Denote by $\ell_1, \ell_2, \ell_3, \ell_4$ the side lengths of Q in cyclic order. Assume first that neither α nor α' take the values $-\infty, \infty$ or 0. Then, up to replacing ℓ_i by $\ell_i^{\alpha'}$, one may assume that $\alpha' = 1$. Write $s = \ell_1 + \ell_3$ and $t = \ell_1^\alpha + \ell_3^\alpha$. Since Q is a 1-quad, we have $\ell_4 = s - \ell_2$. Since Q is also an α-quad, we have

$$\ell_2^\alpha + (s - \ell_2)^\alpha = t, \tag{5.1}$$

and $0 \leq \ell_2 \leq s$. The function $x \mapsto x^\alpha + (s - x)^\alpha$ is strictly monotonic on $[0, s/2]$ and symmetric with respect to $x = s/2$, so that the only solutions of equation (5.1) are $\ell_2 = \ell_1$ and $\ell_2 = \ell_3$. Hence $\{\ell_1, \ell_3\} = \{\ell_2, \ell_4\}$, and Q is a kite.

Assume now that $\alpha = 0$ and α' is finite. One may again assume that $\alpha' = 1$, in which case the sums and products of each pair $\{l_1, l_3\}$ and $\{l_2, l_4\}$ are equal, and Q is again a kite. If $\alpha \in \{-\infty, \infty\}$ and α' is finite non-zero, one may again assume that $\alpha' = 1$ and the conclusion follows easily. The case when $\alpha \in \{-\infty, \infty\}$ and $\alpha' = 0$ is similar. Finally, the case when $\{\alpha, \alpha'\} = \{-\infty, \infty\}$ is also easy. ∎

We finally provide another characterization, involving circumradii of the four triangles delimited by the sides and diagonals of the quad. This last characterization actually holds in a more generic setting, which we now introduce. In what follows, we say that a symmetric function of two variables $f : (\mathbb{R}_+)^2 \to \mathbb{R}$ is *homogeneous* if there exists $u \in \mathbb{R}$ such that for any $\lambda, x, y > 0$, we have $f(\lambda x, \lambda y) = \lambda^u f(x, y)$.

Definition 5.5. Let $f : (\mathbb{R}_+)^2 \to \mathbb{R}$ be a non-constant homogeneous symmetric function of two variables. A quadrilateral $ABCD$ is called an *f-quadrilateral* if

$$f(AB, CD) = f(BC, AD).$$

Multiplying f by a non-zero scalar, or more generally, post-composing it with a bijection, produces the same class of quads. As an example, for $\alpha \in \mathbb{R}^*$, α-quads correspond to the function $f_\alpha\colon (x, y) \mapsto x^\alpha + y^\alpha$. By definition, 0-quads, $+\infty$-quads an $-\infty$-quads are also f-quadrilaterals for some homogeneous function.

Proposition 5.6. *Let $ABCD$ be a quad. Let P denote the intersection point of its diagonals and suppose that P is distinct from A, B, C, D. We denote the respective circumradii of the triangles ABP, BCP, CDP and DAP by R_1, R_2, R_3 and R_4. Let $f\colon (\mathbb{R}_+)^2 \to \mathbb{R}$ be a symmetric homogeneous function. The following are equivalent:*

(1) *$ABCD$ is an f-quadrilateral;*

(2) $f(R_1, R_3) = f(R_2, R_4)$.

This result was already known for orthodiagonal quads and tangential quads [14] and our proof below is a straightforward extension of the proof of [14, Theorem 9].

Proof. Let us denote the centers of the circumcircles of ABP, BCP, CDP, DAP by O_1, O_2, O_3, O_4, respectively. Since AO_1B is isosceles in O_1, we have

$$AB = 2R_1 \sin \frac{\widehat{AO_1B}}{2}.$$

Since P lies on the circle centered at O_1 and going through A and B, we have that

$$\frac{\widehat{AO_1B}}{2} \in \left\{\widehat{APB}, \pi - \widehat{APB}\right\},$$

hence

$$AB = 2R_1 \sin \widehat{APB}.$$

Similarly, we have

$$BC = 2R_2 \sin \widehat{BPC}, \quad CD = 2R_3 \sin \widehat{CPD}, \quad DA = 2R_4 \sin \widehat{DPA}.$$

Observing that $\widehat{APB} = \widehat{CPD} = \pi - \widehat{BPC} = \pi - \widehat{DPA}$, we deduce that the quadruples (AB, BC, CD, DA) and (R_1, R_2, R_3, R_4) are proportional. Since f is homogeneous, $f(AB, CD) = f(BC, DA)$ if and only if $f(R_1, R_3) = f(R_2, R_4)$. This concludes the proof. ∎

Remark 5.7. Let h_1, h_2, h_3 and h_4 be the altitudes through P in the triangles ABP, BCP, CDP and DAP. For $\alpha \in \{1, 2\}$, $ABCD$ is an α-quad if and only if

$$h_1^{-\alpha} + h_3^{-\alpha} = h_2^{-\alpha} + h_4^{-\alpha},$$

see [14, Section 5]. However, this does not hold for general values of α.

We end this section with an open question.

Question 5.8. Apart from f_α, are there homogeneous functions f such that f-quadrilaterals satisfy one of the flip properties discussed in this paper?

A. Jacobi elliptic functions

In this appendix, we give a very brief presentation of elliptic functions and formulas used in the paper, with variable names that are not classical but fit the framework of our paper. For a more complete introduction, we refer to [1, 23].

Consider a number $k \in [0,1) \cup i\mathbb{R}$, which we call *elliptic modulus*. We first define the *incomplete integral of the first kind*:

$$F(\theta, k) = \int_0^\theta \frac{dt}{\sqrt{1 - k^2 \sin^2 t}}.$$

The function $F(\cdot, k)$ is a bijection from $\mathbb{R}$ to $\mathbb{R}$, and we denote its inverse by $\mathrm{am}(\cdot, k)$. Then the first two Jacobi elliptic functions are defined for any $\tau \in \mathbb{R}$ by

$$\mathrm{cn}(\tau, k) = \cos(\mathrm{am}(\tau, k)), \quad \mathrm{sn}(\tau, k) = \sin(\mathrm{am}(\tau, k)).$$

These functions can be thought of as generalizations of usual cosine and sine functions. For $k = 0$, the function $F(\cdot, k)$ is clearly the identity, hence cn and sn reduce to cos and sin. In general, they are periodic functions, of period $4K(k)$ where K denotes the *complete integral of the first kind*, also named *quarter-period*:

$$K(k) = F\Big(\frac{\pi}{2}, k\Big).$$

Apart from cn and sn, we also define

$$\mathrm{dn}(\tau, k) = \sqrt{1 - k^2 \,\mathrm{sn}(\tau, k)}.$$

Then, for any two distinct letters $p, q \in \{c, s, d, n\}$, we define a function pq as $\frac{pn}{qn}$, with the convention that $nn = 1$. For instance,

$$\mathrm{nc}(\tau, k) = \frac{1}{\mathrm{cn}(\tau, k)}, \quad \mathrm{sc}(\tau, k) = \frac{\mathrm{sn}(\tau, k)}{\mathrm{cn}(\tau, k)},$$

etc.

The following formulas, which can be found in [1, Chapter 16.8], describe how these elliptic functions are affected by the change of variable $\tau \mapsto K(k) - \tau$. As is customary, we omit the dependence in k to simplify notations. Letting $k' = \sqrt{1 - k^2}$, one has

$$\mathrm{cn}(K - \tau) = k' \,\mathrm{sd}(\tau), \quad \mathrm{sn}(K - \tau) = \mathrm{cd}(\tau), \quad \mathrm{dn}(K - \tau) = k' \,\mathrm{nd}(\tau). \qquad \text{(A.1)}$$

The effect of the same change of variable on any other function pq can be deduced from these three.

We also make use of an addition identity, that can be found in [23, Chapter 2, p. 48, 32 (i)]. For any $\tau, \tau' \in \mathbb{R}$,

$$\operatorname{cn}(\tau + \tau') + \operatorname{sn}(\tau)\operatorname{sn}(\tau')\operatorname{dn}(\tau + \tau') - \operatorname{cn}(\tau)\operatorname{cn}(\tau') = 0. \tag{A.2}$$

Acknowledgments. We are grateful to Dmitry Chelkak, Marianna Russkikh and Andrea Sportiello for numerous fruitful discussions. We also thank Thomas Blomme and Othmane Safsafi for discussions leading to the proof of Propositions 5.4 and 5.6. We thank the referees for comments leading to an improved exposition.

Funding. P. Melotti and S. Ramassamy are partially supported by the Agence Nationale de la Recherche, Grant no. ANR-18-CE40-0033 (ANR DIMERS). S. Ramassamy also acknowledges the support of the Fondation Sciences Mathématiques de Paris. P. Thévenin acknowledges partial support from Agence Nationale de la Recherche, Grant no. ANR-14-CE25-0014 (ANR GRAAL).

References

[1] M. Abramowitz and I. A. Stegun, *Handbook of mathematical functions with formulas, graphs, and mathematical tables*. National Bureau of Standards Applied Mathematics Series 55, U. S. Government Printing Office, Washington, D.C., 1964 Zbl 0171.38503 MR 0167642

[2] E. J. Atzema, A theorem by Giusto Bellavitis on a class of quadrilaterals. *Forum Geom.* **6** (2006), 181–185 Zbl 1133.51010 MR 2282234

[3] R. J. Baxter, *Exactly solved models in statistical mechanics*. Academic Press, London, 1982 Zbl 0538.60093 MR 690578

[4] N. Berger and M. Biskup, Quenched invariance principle for simple random walk on percolation clusters. *Probab. Theory Related Fields* **137** (2007), no. 1–2, 83–120 Zbl 1107.60066 MR 2278453

[5] C. Boutillier, B. de Tilière, and K. Raschel, The Z-invariant Ising model via dimers. *Probab. Theory Related Fields* **174** (2019), no. 1–2, 235–305 Zbl 1419.82008 MR 3947324

[6] D. Chelkak, Ising model and s-embeddings of planar graphs. 2020, arXiv:2006.14559, to appear in *Ann. Sci. Éc. Norm. Supér. (4)*

[7] D. Chelkak, Planar Ising model at criticality: state-of-the-art and perspectives. In *Proceedings of the International Congress of Mathematicians – Rio de Janeiro 2018, Vol. IV, Invited lectures*, pp. 2801–2828, World Scientific Publishing, Hackensack, NJ, 2018 Zbl 1453.82006 MR 3966512

[8] D. Chelkak and S. Smirnov, Discrete complex analysis on isoradial graphs. *Adv. Math.* **228** (2011), no. 3, 1590–1630 Zbl 1227.31011 MR 2824564

[9] D. Chelkak and S. Smirnov, Universality in the 2D Ising model and conformal invariance of fermionic observables. *Invent. Math.* **189** (2012), no. 3, 515–580 Zbl 1257.82020 MR 2957303

[10] J. Dubédat, Exact bosonization of the Ising model. 2011, arXiv:1112.4399

[11] H. Duminil-Copin, J.-H. Li, and I. Manolescu, Universality for the random-cluster model on isoradial graphs. *Electron. J. Probab.* **23** (2018), paper no. 96 Zbl 1414.60076 MR 3858924

[12] G. R. Grimmett and I. Manolescu, Bond percolation on isoradial graphs: criticality and universality. *Probab. Theory Related Fields* **159** (2014), no. 1–2, 273–327 Zbl 1296.60263 MR 3201923

[13] M. Josefsson, When is a tangential quadrilateral a kite? *Forum Geom.* **11** (2011), 165–174 Zbl 1285.51014 MR 2877272

[14] M. Josefsson, Characterizations of orthodiagonal quadrilaterals. *Forum Geom.* **12** (2012), 13–25 Zbl 1242.51009 MR 2955646

[15] S. Kakutani, Markoff process and the Dirichlet problem. *Proc. Japan Acad.* **21** (1945), no. 1, 227–233 Zbl 0063.03110 MR 32866

[16] A. E. Kennelly, The equivalence of triangles and three-pointed stars in conducting networks. *Electr. World and Eng.* **34** (1899), no. 12, 413–414

[17] R. Kenyon, An introduction to the dimer model. In *School and Conference on Probability Theory*, pp. 267–304, ICTP Lect. Notes 17, The Abdus Salam International Centre for Theoretical Physics, Trieste, 2004 Zbl 1076.82025 MR 2198850

[18] R. Kenyon, W. Y. Lam, S. Ramassamy, and M. Russkikh, Dimers and circle patterns. *Ann. Sci. Éc. Norm. Supér. (4)* **55** (2022), no. 3, 865–903 Zbl 1497.82007

[19] R. Kenyon and R. Pemantle, Principal minors and rhombus tilings. *J. Phys. A* **47** (2014), no. 47, paper no. 474010 Zbl 1310.15011 MR 3280001

[20] R. Kenyon and R. Pemantle, Double-dimers, the Ising model and the hexahedron recurrence. *J. Combin. Theory Ser. A* **137** (2016), 27–63 Zbl 1325.05136 MR 3403514

[21] B. G. Konopelchenko and W. K. Schief, Reciprocal figures, graphical statics, and inversive geometry of the Schwarzian BKP hierarchy. *Stud. Appl. Math.* **109** (2002), no. 2, 89–124 Zbl 1114.37305 MR 1917041

[22] H. A. Kramers and G. H. Wannier, Statistics of the two-dimensional ferromagnet. Part I. *Phys. Rev.* **60** (1941), no. 3, 252–262 Zbl 0027.28505 MR 4803

[23] D. F. Lawden, *Elliptic functions and applications*. Appl. Math. Sci. 80, Springer, New York, 1989 Zbl 0689.33001 MR 1007595

[24] M. Lis, Circle patterns and critical Ising models. *Comm. Math. Phys.* **370** (2019), no. 2, 507–530 Zbl 1426.82011 MR 3994578

[25] D. Lucarelli, A. Saksena, R. Farrell, and I.-J. Wang, Distributed inference for network localization using radio interferometric ranging. pp. 52–73, Lecture Notes in Comput. Sci. 4913, Springer, Berlin, 2008

[26] L. Onsager, Crystal statistics. I. A two-dimensional model with an order-disorder transition. *Phys. Rev.* **65** (1944), no. 3–4, 117–149 Zbl 0060.46001 MR 10315

[27] W. T. Tutte, How to draw a graph. *Proc. Lond. Math. Soc. (3)* **13** (1963), no. 1, 743–767 Zbl 0115.40805 MR 158387

[28] G. H. Wannier, The statistical problem in cooperative phenomena. *Rev. Modern Phys.* **17** (1945), no. 1, 50–60

[29] H. Whitney, 2-isomorphic graphs. *Amer. J. Math.* **55** (1933), no. 1–4, 245–254 Zbl 0006.37005 MR 1506961

[30] X. Xu, S. Sahni, and N. S. V. Rao, On basic properties of localization using distance-difference measurements. In *Proceedings of 11th International Conference on Information Fusion*, pp. 123–130, IEEE, 2008

Communicated by Adrian Tanasă

Received 19 February 2021; revised 11 August 2021.

Paul Melotti
Université Paris-Saclay, CNRS, Laboratoire de mathématiques d'Orsay, 91405 Orsay, France; paul.melotti@universite-paris-saclay.fr

Sanjay Ramassamy
Université Paris-Saclay, CNRS, CEA, Institut de Physique Théorique, 91191 Gif-sur-Yvette, France; sanjay.ramassamy@ipht.fr

Paul Thévenin
Department of Mathematics, Uppsala Universitet, Lägerhyddsvägen 1, 75237 Uppsala, Sweden; paul.thevenin@math.uu.se